NASA TECHNICAL NOTE

NASA TN D-2934

NASA TN D-2934

ANALYTICAL AND EXPERIMENTAL STUDY OF NUCLEAR HEATING OF LIQUID HYDROGEN

by Bernhard H. Anderson and Ronald L. Danilowicz

Lewis Research Center
Cleveland, Ohio

NATIONAL AERONAUTICS AND SPACE ADMINISTRATION • WASHINGTON, D. C. • JULY 1965

ANALYTICAL AND EXPERIMENTAL STUDY OF NUCLEAR HEATING OF LIQUID HYDROGEN

By Bernhard H. Anderson and Ronald L. Danilowicz

Lewis Research Center
Cleveland, Ohio

NATIONAL AERONAUTICS AND SPACE ADMINISTRATION

For sale by the Clearinghouse for Federal Scientific and Technical Information
Springfield, Virginia 22151 – Price $2.00

ANALYTICAL AND EXPERIMENTAL STUDY OF NUCLEAR HEATING OF LIQUID HYDROGEN

by Bernhard H. Anderson and Ronald L. Danilowicz

Lewis Research Center

SUMMARY

As part of the overall study of the behavior of propellants contained in space vehicle tanks, an analytical and experimental investigation was conducted to determine the effects of nuclear heat generation on the temperature history of any point in the tank. In the experiments, which were performed in a 125-gallon tank positioned over a nuclear reactor, both the tank walls and the liquid hydrogen were heated by nuclear radiation. Experiments were performed where the total heating rate was varied from 177 to approximately 1000 watts. Experimental data were obtained over a range of flow discharge rates from 0.04 to 0.13 pound per second and ullage pressures of 30 to 60 pounds per square inch absolute.

The results of this investigation showed that a portion of the nuclear heating generated within the tank walls caused convective motion of the hydrogen, which carried warm fluid to the liquid surface and formed a temperature gradient or stratified layer. In general, no gross changes in the flow behavior were observed over the range of test parameters.

An approximate analysis was developed to predict the local temperature rise in a subcooled fluid, subjected to wall heating and internal absorption of energy, and discharging at constant flow rate and pressure. Comparisons between experiment and analysis indicate that the analysis can predict the temperature histories with reasonable accuracy.

A study was made to determine the effects that the various analytical assumptions in the assumed flow model have on the calculated temperature history. Within the range of experimental test parameters, no appreciable error was introduced by considering the flow along the side walls to develop in a manner similar to the development of flow along a semi-infinite vertical flat plate. The position on the tank wall at which the boundary layer was assumed to initiate was arbitrarily varied to investigate its influence on the temperature profile in the tank. All of the heating below this position was assigned to bulk heating. The results indicate that varying this position had little effect on the temperature histories.

INTRODUCTION

A knowledge of the effects of heating a cryogenic propellant is important to the optimization of components in a nuclear space vehicle because it determines, in part, the selection of pumps, insulation, shielding, venting devices, and tank construction. The study of propellant heating, however, necessitates an examination of several related physical phenomena, such as (1) pressurization, (2) interfacial mass and energy transfer, and (3) thermal stratification. This report deals primarily with the problem of thermal stratification and the resultant temperature histories. Thermal stratification results from the natural convection flow of fluid along the side walls of the tank into the upper region near the gas-liquid interface. The warm fluid accumulates near the surface and forms a stable temperature gradient. Within a radiation field, such as would be encountered in a nuclear vehicle, thermal stratification may be affected by large amounts of internal absorption of energy near the tank bottom. This type of heating is inherently unstable and gives rise to turbulent mixing that may alter the flow induced by heating the tank walls.

Relatively little information is available on the natural convection flow of a completely confined fluid subjected to bottom heating or internal absorption of energy in addition to wall heating. One of the first studies to describe the resulting flow behavior experimentally is reported in reference 1, where small-scale tests were performed using infrared radiation as the energy source. It was shown in reference 1 that the complete-mix theory can predict the temperature rise of a subcooled fluid, exposed to internal heat generation alone. When wall heating is present, however, complete-mix calculations are no longer applicable because thermal gradients are formed at the liquid surface. Several researchers in the field have sought refined analytical methods to predict the temperature gradients in the fluid resulting from wall heating. One of the earlier analyses to account for the effects of wall heating is presented in reference 2. In this reference, a convective-flow model is postulated that is primarily concerned with the development of stratification for a nondraining (self-pressurizing) system. Other approximate analyses, which are also concerned with this problem, are presented in references 3 and 4, each of which uses a numerical approach. The gradients in the liquid were considered to develop in finite step increments, where the amount of heat associated with each increment was determined from vertical-flat-plate natural-convection solutions developed by Eckert and Jackson (ref. 5). Reference 4 incorporates the effects of nuclear heat generation in addition to the effects of wall heating; however, no comparisons are made with experimental data. An excellent review article that discusses the various approaches to this problem appears in reference 6.

This report investigates the effects of nuclear heat generation on temperature histories of any point in liquid hydrogen contained in a tank, both analytically and experimentally. The basic approach taken in the analysis differed from those in references 3 and 4 in that a similarity profile (the dimensionless temperature profile is independent of the spacial coordinate) is postulated which is made to satisfy conservation of energy. The analysis was first presented in summary form in reference 7. Experimental data obtained in a nuclear environment for NASA under contract with General Dynamics Corp., Fort Worth, Texas (ref. 8) are analyzed and discussed. Problems associated with interpreting the experimental results are discussed, and some of the analytical

assumptions are examined to establish their validity within the range of applicability.

ANALYSIS

The problem to be considered here is that of determining the temperature distribution in a subcooled fluid (liquid hydrogen) resulting from wall heating and internal absorption of energy. This class of problems is characterized by the condition that the Grashof number is high; that is, the product of the buoyancy times the inertial forces of the system is large in comparison with the viscous forces involved.

It is well known from boundary-layer theory that, as the Grashof number becomes large, without any other changes in the flow field, the region of fluid, in which the viscous forces are large (near the fluid boundaries), becomes smaller and ultimately reduces to a thin layer or boundary layer (ref. 9). For the flow in a confined space, however, the analysis is not simplified by the conventional boundary approximations to yield a flow that is separated into a viscous (boundary layer) region and an inviscid region where the flow is known. For the case of flow in a confined space, the interior flow outside the boundary layer depends on the flow in the boundary layer because motion originates in the boundary layer where there are density variations (ref. 10). The departure from classical boundary-layer theory, for those classes of problems in which the fluid is completely confined, is thus seen to come about because of the coupling between the exterior and boundary-layer flows.

The formulation of the flow model in this analysis will be highly idealized in the sense that a flat-plate natural-convection boundary-layer solution will be used. This precludes, therefore, any coupling between interior and boundary-layer flow.

Formulation of Analytical Flow Model

It was pointed out in reference 1 that, when nonuniform source heating acts in conjunction with wall heating (heat transfer from the tank walls), two distinct regions are developed. In the lower region, in which fluid is in a state of agitated mixing, there is a uniform temperature profile. In the upper region, a temperature gradient is formed that is caused by the accumulation of warm fluid from the boundary layer along the tank walls. This qualitative description is the basic foundation of the analytical flow model and is shown schematically in figure 1. The region below the temperature gradient is termed the region of bulk heating and is separated from the upper region or "stratified layer" by the position x_o, where x is measured in the axial direction from the tank bottom. The position of the liquid surface is called x_s and is a function of time; that is, $x_s = x_s(t)$. (All symbols are defined in appendix A.) The system is considered to include only the fluid in the tank, which is discharging at constant pressure and constant flow rate. The boundary conditions include the wall-heating distribution and the surface temperature, which depends on the ullage pressure. In addition, heat is being added to the

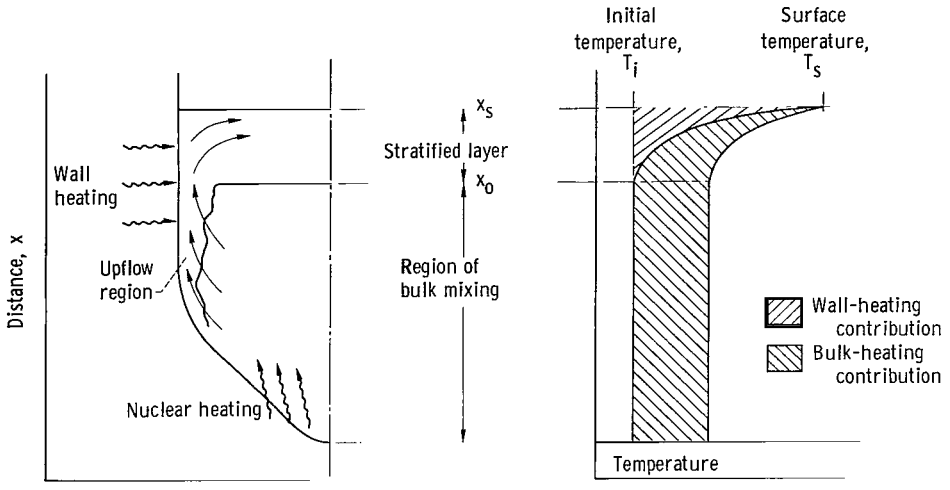

Figure 1. - Schematic diagram of analytical flow model.

system by the absorption of nuclear radiation.

In order to simplify the analysis, while retaining some of the essential features of the problem, the following assumptions are made:

(1) The heat that is distributed within the hydrogen is considered to have its origin from two sources: heat transfer from the tank walls and heating induced by the absorption of nuclear radiation.

(2) The fluid is considered to discharge at constant ullage pressure with no heat or mass transfer across the gas-liquid interface.

(3) The liquid surface is at saturation temperature corresponding to the ullage pressure.

(4) The heat input to the fluid does not vary in the radial or circumferential directions.

Assumptions (1) and (2) establish the class of problems under consideration where the heat transfer from the walls and from the absorption of nuclear radiation constitute the major source of heat input to the fluid, which is discharging at constant pressure and where there is negligible mass transfer across the liquid surface (ref. 11). In assumption (3), it is further assumed that the liquid surface is in equilibrium with the ullage gas. Assumption (4) establishes the fact that only symmetrical heating is considered in the problem.

It was indicated in reference 1 that, with a "bulk" temperature that is varying with time, the temperature profiles in the "stratified layer" appear to exhibit the property of similarity, defined here as the property that two temperature profiles $\vartheta(x,t)$ at different times t differ only by a scale factor in x and ϑ. The temperature defined by ϑ is the temperature difference $(T(x,t))$ from the initial temperature (T_i). The thickness of the stratified δ and the temperature difference across the stratified layer $\vartheta_s(t) - \vartheta_b(t)$ from

reference 1 proved to be usable scale parameters. The dimensionless temperature profile (see eq. (3) of ref. 1) can be written as

$$\frac{\vartheta(x,t) - \vartheta_b(t)}{\vartheta_s(t) - \vartheta_b(t)} = \Psi\left(\frac{x - x_o}{\delta}\right)$$

where $\Psi[(x - x_o)/\delta]$ is an appropriate function of the argument $(x - x_o)/\delta$ in which both x_o and δ are functions of time. The ratio of bulk temperature rise $\vartheta_b(t)$ to the saturation temperature rise $\vartheta_s(t)$ can be expressed as some function of time; that is,

$$\frac{\vartheta_b(t)}{\vartheta_s(t)} = f(t) \tag{1}$$

Using equation 1 gives the temperature in the stratified layer as

$$\vartheta(x,t) = \vartheta_s(t)\left\{f(t)\left[1 - \Psi\left(\frac{x - x_o}{\delta}\right)\right] + \Psi\left(\frac{x - x_o}{\delta}\right)\right\}$$

The function $[\Psi\ (x - x_o)/\delta]$ will now be assumed to have the form

$$\Psi\left(\frac{x - x_o}{\delta}\right) = \left(\frac{x - x_o}{\delta}\right)^n$$

Thus, the temperature in the stratified layer can be written as

$$\vartheta(x,t) = \vartheta_s(t)\left\{f(t)\left[1 - \left(\frac{x - x_o}{\delta}\right)^n\right] + \left(\frac{x - x_o}{\delta}\right)^n\right\} \tag{2}$$

By assumption (2) $\vartheta_s(t) = T_s - T_i$ becomes a constant that is determined by the ullage pressure and the initial temperature. The term $f(t)\left[1 - \left(\frac{x - x_o}{\delta}\right)^n\right]$ can be interpreted as the necessary contribution of bulk heating to the stratified layer to satisfy the similarity condition. With no bulk heating $f(t) = 0$ and $\vartheta_b(t)$ vanishes giving $T_s - T_i$ as the scaling parameter for the temperature in the stratified layer.

A schematic representation of the temperature in the tank appears in figure 1. At the liquid surface $x = x_s$, the bulk heating contribution vanishes, and the temperature becomes $T(x_s,t) = T_s$. At the lower extremity of the stratified layer $x = x_o$, only the bulk heating contributes to the rise in temperature and $T(x_o,t) = T_i + (T_s - T_i)f(t)$.

Growth of Stratified Layer

To determine the growth parameter δ and the exponent n that appear in equation (2), the following additional assumptions will be made:

(5) The resulting temperature distribution does not vary in the radial or circumferential direction.

(6) The physical properties of the fluid do not vary appreciably over the temperature range under consideration.

Assumption (5) appears to be justified everywhere except within a thin region near the tank wall where a boundary layer exists. This assumption is valid when the dimensions of the tank are large in comparison with the thickness of the wall boundary layer and when the Prandtl number is close to 1, as is the case with liquid hydrogen. Based on assumption (6), fluid properties evaluated at an average temperature are used.

The expression for the mass of fluid entering the stratified layer can be described by an energy balance between the boundary layer and the wall heating in the form

$$\frac{dm}{dt} = \frac{1}{c_p \bar{\theta}} \int_0^{x_o(t)} q_w \frac{d\sigma}{dx} dx \tag{3}$$

where $\bar{\theta}$ and dm/dt are the average temperature difference and mass flow of fluid entering the stratified layer, respectively, and σ is the surface area of the tank. The energy balance equation for the system expresses the fact that the time rate of increase of enthalpy of the fluid plus the rate at which enthalpy is being transported out of the system is equal to the total rate of heat entering the system considering an arbitrary tank geometry. The energy equation for the system can be written as

$$\rho c_p \frac{d}{dt} \int_0^{x_s(t)} \vartheta(x,t) A(x) dx + c_p \dot{w}_p \vartheta(0,t)$$

$$= \int_0^{x_s(t)} q_w(x) \frac{d\sigma}{dx} dx + \int_0^{x_s(t)} q_n(x) A(x) dx \tag{4}$$

where $x_s(t)$ is the location of the liquid surface and $\vartheta(x,t)$ is the temperature of the fluid minus the initial temperature that can be expressed from equation (2)

$$\vartheta(x,t) = \vartheta_s \left[f(t)\varphi(x,t) + \psi(x,t) \right] \tag{5}$$

and the functions $\psi(x,t)$ and $\varphi(x,t)$ can be written explicitly as

$$\left.\begin{aligned}
\psi(x,t) &= \left[\frac{x - x_o(t)}{\delta(t)}\right]^n \qquad x_o(t) \le x \le x_s(t) \\
\psi(x,t) &= 0 \qquad 0 \le x \le x_o(t) \\
\varphi(x,t) &= 1 - \left[\frac{x - x_o(t)}{\delta(t)}\right]^n \qquad x_o(t) \le x \le x_o(t) \\
\varphi(x,t) &= 1 \qquad 0 \le x < x_s(t)
\end{aligned}\right\} \tag{6}$$

Introducing the liquid level x_s as the independent variable through the transformation

$$x_s = L - \int_0^t \frac{\dot{w}_p}{\rho A}(x_s)dt$$

gives equations (3) and (4) as

$$\frac{dm}{dx_s} = -\frac{\rho A(x_s)}{c_p \dot{w}_p \bar{\theta}} \int_0^{x_o(t)} q_w(x)\,\frac{d\sigma}{dx}\,dx$$

$$\frac{d}{dx_s}\int_0^{x_s} \vartheta(x,x_s)A(x)dx - \vartheta(0,x_s)A(x_s) = -\frac{A(x_s)}{c_p \dot{w}_p}\left[\int_0^{x_s} q_w(x)\,\frac{d\sigma}{dx}\,dx + \int_0^{x_s} q_n(x)A(x)dx\right]$$

By equating the mass flow rate entering the stratified layer to the rate of growth of the layer, the volumetric growth becomes

$$\frac{d}{dx_s}\int_{x_o}^{x_s} A(x)dx = -\frac{A(x_s)}{c_p \dot{w}_p \bar{\theta}} \int_0^{x_o} q_w(x)\,\frac{d\sigma}{dx}\,dx \tag{7}$$

Introducing equation (5) into the energy equation for the system and assuming that the contributions of wall and internal heating can be uncoupled with the appropriate change of variable result in the following equations:

$$\frac{d}{dx_s}\int_0^{x_s} \psi(x,x_s)A(x)dx = -\frac{A(x_s)}{c_p \dot{w}_p \vartheta_s} \int_0^{x_s} q_w(x)\,\frac{d\sigma}{dx}\,dx \tag{8}$$

$$\frac{d}{dx_s}\int_0^{x_s} f(x_s)\varphi(x,x_s)A(x)dx - f(x_s)A(x_s) = -\frac{A(x_s)}{c_p\dot{w}_p\vartheta_s}\int_0^{x_s} q_n(x)A(x)dx \tag{9}$$

Differentiating the left side of equation (7), noting that $x_o = x_s - \delta(x_s)$, gives

$$A(x_s) - A(x_o)\left(1 - \frac{d\delta}{dx_s}\right) = -\frac{A(x_s)}{c_p\dot{w}_p\overline{\theta}}\int_0^{x_o} q_w(x)\,\frac{d\sigma}{dx}\,dx \tag{10}$$

The left side of equation (8) can be integrated successively by parts, thus

$$\frac{d}{dx_s}\left\{\frac{\delta(x_s)A(x_s)}{(n+1)} - \frac{\delta^2(x_s)\,\frac{d}{dx_s}\left[A(x_s)\right]}{(n+1)(n+2)} + \frac{\delta^3(x_s)\,\frac{d^2}{dx_s^2}\left[A(x_s)\right]}{(n+1)(n+2)(n+3)} - \cdots\right\}$$

$$= -\frac{A(x_s)}{c_p\dot{w}_p\vartheta_s}\int_0^{x_s} q_w(x)\,\frac{d\sigma}{dx}\,dx \tag{11}$$

Consider now equations (10) and (11) in the limit as the liquid level x_s approaches its initial value L. Noting that the limit $\delta(x_s) = 0$ gives $x_s \to L$

$$\frac{d\delta}{dx_s} = -\frac{1}{c_p\dot{w}_p\overline{\theta}}\int_0^{L} q_w(x)\,\frac{d\sigma}{dx}\,dx$$

$$\frac{d\delta}{dx_s} = -\frac{(n+1)}{c_p\dot{w}_p\vartheta_s}\int_0^{L} q_w(x)\,\frac{d\sigma}{dx}\,dx$$

Solving for the exponent n from the preceding equations gives

$$n = \frac{\vartheta_s}{\overline{\theta}} - 1 \tag{12}$$

In the limit as x_s approaches the initial liquid level L, the exponent n becomes independent of tank geometry. The a posteriori assumption is now made that the exponent n, defined by equation (12), represents a valid first-order approximation at some later time.

At large Grashof numbers, the flow near the tank walls has the character of a boundary-layer flow coupled to the interior flow. To simplify the analy-

sis, the assumption is made that temperature rise which contributes to the "main bulk" from this coupling (see fig. 1) is small relative to nuclear heating. The definition of the average temperature $\overline{\theta}$ is implied from equation (3) and is given by

$$\overline{\theta} = \frac{\int_0^{\Delta} \theta(u + u_o)(R - y)dy}{\int_0^{\Delta} (u + u_o)(R - y)dy}$$

where θ is the temperature in the boundary layer relative to the bulk temperature, u and u_o are the velocities in the boundary layer and of the interface, x_o, between the stratified layer and the bulk, y is the coordinate normal to the tank wall, Δ is the thickness of the boundary layer, and R is the radius of the tank. In effect, the average temperature $\overline{\theta}$ is the ratio of the energy to the mass flux entering the stratified layer relative to a coordinate system moving with velocity u_o. Both the mass flux and the energy flux entering the stratified layer are evaluated in appendix B, with the assumption that the turbulent free-convection profiles (ref. 5),

$$u = u_1\left(\frac{y}{\Delta}\right)^{1/7}\left(1 - \frac{y}{\Delta}\right)^4$$

$$\theta = \theta_w\left[1 - \left(\frac{y}{\Delta}\right)^{1/7}\right]$$

can be used to represent the flow in the boundary layer. For Grashof numbers of the order of 10^{14} (typical for liquid hydrogen), the zeroth order approximation

$$\overline{\theta} = \frac{\int_0^{\Delta} u\theta \, dy}{\int_0^{\Delta} u \, dy} = 0.250 \, \theta_w \tag{13}$$

gives results that are accurate within 1.5 percent. It should be noted, however, that the mass and energy flux terms, individually, can vary appreciably from the zeroth order approximation even at Grashof numbers of the order of 10^{14}.

To obtain equation (13), the governing equations were treated under the highly idealized concept of the flow originating from a steady-state condition at time zero, thus ignoring the starting transients. From equations (12) and (13), the initial value of the exponent n becomes

$$n = 4.00 \frac{\vartheta_s}{\vartheta_w} - 1 \tag{14}$$

Equations (11) and (14) are used to evaluate the growth parameter $\delta(x_s)$ of the stratified layer. By formulating the mathematical problem in this manner, only the parameter n contains boundary-layer effects. Thus, as can be seen from equation (11), the growth parameter $\delta(x_s)$ will always adjust itself to satisfy conservation of energy for the wall-heating portion of the total heat. Then the flexibility of determining departures from flat-plate solutions without violating conservation of energy for the system is permitted.

The lower extremity of the stratified layer is given by the relation

$$x_o = x_s - \delta(x_s)$$

where $\delta(x_s)$ is evaluated from equations (11) and (14). The period of growth of the layer can now be explicitly defined as $0 \leq x_o \leq x_s$, which hereinafter is called the initial period. The location of the liquid surface when $x_o = 0$ is defined as $x_{s,l}$; the later period is defined as $0 < x_s < x_{s,l}$.

Temperature Distribution in Initial Period

The parameter $f(x_s)$, or $f(t)$, that appears in equation (5) can now be obtained from equation (9). Thus, after simplification, equation (9) becomes

$$\frac{df}{dx_s}\int_0^{x_s} \varphi(x,x_s)A(x)dx - f\frac{d}{dx_s}\int_0^{x_s} \psi(x,x_s)A(x)dx = -Q_n(x_s)$$

where

$$Q_n(x_s) = \frac{A(x_s)}{c_p\dot{w}_p\vartheta_s}\int_0^{x_s} q_n(x)A(x)dx$$

Let

$$a(x_s) = \int_0^{x_s} \varphi(x,x_s)A(x)dx \tag{15}$$

and

$$b(x_s) = \frac{d}{dx_s}\int_0^{x_s} \psi(x,x_s)A(x)dx \tag{16}$$

the governing equation then becomes

$$a(x_s)\frac{df}{dx_s} - b(x_s)f = -Q_n(x_s) \tag{17}$$

The function $f(t)$, or $f(x_s)$, that appears in equation (5) can now be determined from the solution of equation (17) together with the initial condition $f(L) = 0$, where L is the initial liquid level. The evaluations of the parameters $a(x_s)$ and $b(x_s)$ are discussed in appendix C.

Temperature Distribution in Later Period

As mentioned, the later period begins after the exit port first experiences the presence of the stratified layer. During this period, a temperature rise is seen at the exit port due to the temperature profile being "carried" with the fluid during discharge in addition to the heat being added to the system. To account for both of these processes, the temperature function $\vartheta(x,x_s)$ is postulated now to have the form

$$\vartheta(x,x_s) = \vartheta_s\left[F(x_s)\Phi(x,x_s) + \Psi(x,x_s)\right] \tag{18}$$

where

$$\Psi(x,x_s) = \left(1 - \frac{x_s - x}{x_{s,l}}\right)^n \qquad 0 \le x \le x_s \tag{19}$$

$$\Phi(x,x_s) = 1 - \left(1 - \frac{x_s - x}{x_{s,l}}\right)^n \qquad 0 \le x \le x_s \tag{20}$$

Equation (18) satisfies the condition that, at $x_s = x_{s,l}$ the temperature profiles are matched provided that $F(x_{s,l}) = f(x_{s,l})$. Introducing equation (18) into equation (4), with the appropriate change of variable, yields

$$\frac{d}{dx_s}\int_0^{x_s} F(x_s)\Phi(x,x_s)A(x)dx + \frac{d}{dx_s}\int_0^{x_s} \Psi(x,x_s)A(x)dx - F(x_s)\Phi(0,x_s)A(x_s)$$

$$- \Psi(0,x_s)A(x_s) = - Q_w(x_s) - Q_n(x_s) \tag{21}$$

where

$$Q_w(x_s) = \frac{A(x_s)}{c_p\dot{w}_p\vartheta_s}\int_0^{x_s} q_w(x)\,\frac{d\sigma}{dx}\,dx \tag{22}$$

$$Q_n(x_s) = \frac{A(x_s)}{c_p\dot{w}_p\vartheta_s}\int_0^{x_s} q_n(x)A(x)dx \tag{23}$$

Equation (21) can be simplified to the form

$$\alpha(x_s)\,\frac{dG}{dx_s} - \gamma(x_s)G = Q(x_s) \tag{24}$$

where

$$\alpha(x_s) = \int_0^{x_s} \Phi(x,x_s)A(x)dx = \int_0^{x_s} A(x)dx - \int_0^{x_s} \Psi(x,x_s)A(x)dx \qquad (25)$$

$$\gamma(x_s) = \frac{d}{dx_s}\int_0^{x_s} \Psi(x,x_s)A(x)dx - \Psi(0,x_s)A(x_s) \qquad (26)$$

$$G(x_s) = 1.0 - F(x_s) \qquad (27)$$

$$Q(x_s) = Q_w(x_s) + Q_n(x_s) \qquad (28)$$

Equation (24) together with the initial condition that $G(x_{s,l}) = 1.0 - f(x_{s,l})$ comprises the mathematical formulation of the problem in the later period. See appendix D for the evaluations of the integrals:

$$\int_0^{x_s} \Psi(x,x_s)A(x)dx$$

and

$$\frac{d}{dx_s}\int_0^{x_s} \Psi(x,x_s)A(x)dx$$

SUMMARY OF ANALYSIS

The temperature history at any point in the tank can be computed from equation (5) for the initial period $0 \leq x_o \leq x_s$ and from equation (18) for the later period $0 \leq x_s < x_{s,l}$. The functions $f(x_s)$ and $F(x_s)$ that appear in equations (5) and (18), respectively, are determined from the solution of the first-order linear differential equations (17) and (24). The variable coefficients that appear in these equations are functions of n and δ, which can be determined from equations (14) and (11), respectively.

Other variables that must be known before solution can be obtained are the input parameters: specific heat c_p, flow rate $\dot{w}_p$, saturation temperature minus initial temperature ϑ_s, density ρ, the wall heat distribution $q_w(x)$, and the nuclear or internal distribution of heat $q_n(x)$, and the tank geometry. The specific heat and fluid density should be determined from an average temperature during discharge. An average temperature rise can be obtained by first basing the values of c_p and ρ on the initial temperature and computing a temperature history. From this temperature history, an average temperature over the time to discharge can be determined from which new values of c_p and ρ can be obtained. By iterating in this manner, usable values of specific heat and density can be obtained without prior knowledge of the temperature history.

The parameter θ_w that appears in equation (14) can be obtained by using

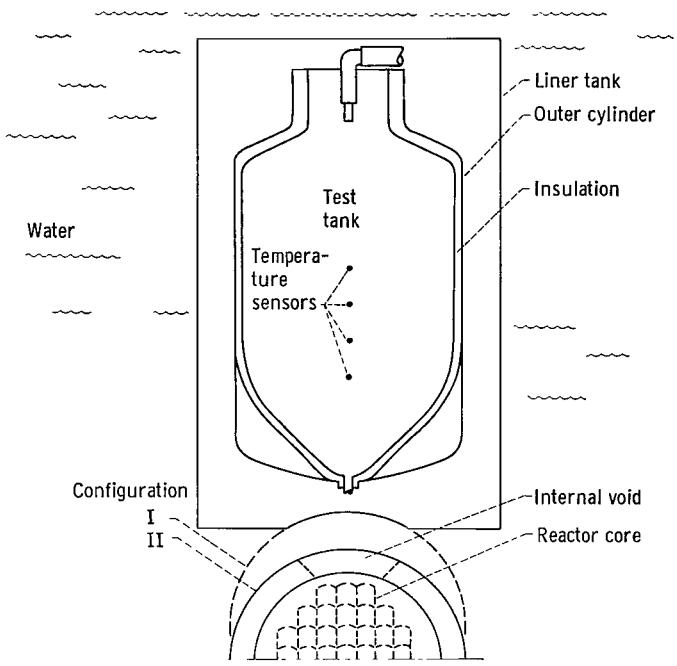

Figure 2. - Nuclear tank-heating experiment.

an average wall heat flux together with a heat-transfer equation relating wall heat flux to wall temperature. The constant multiplying the term ϑ_s/θ_w in equation (14) comes about by using the turbulent free-convection profile presented in reference 5. This constant can be arbitrarily varied, without violating conservation of energy for the system, in order to correct for the idealization of the wall boundary development empirically, that is, as if it were developing along a semi-infinite vertical flat plate.

NUCLEAR RADIATION EXPERIMENTS

Tests were conducted to obtain propellant heating data with a nuclear reactor as the energy source (ref. 8). The experimental equipment and test parameters were chosen by scaling from a typical nuclear rocket vehicle, with a capacity of 100 000 pounds of propellant. The value of flow rate for some of the runs was chosen to yield the same time to outflow as the nuclear rocket. Other tests were conducted in which the value of flow rate was varied to study the induced temperature distributions as a function of flow rate. Heating rates in the propellant of a nuclear rocket depend on the particular vehicle geometry, shielding, and placement of equipment, and as such cannot be determined until a vehicle is exactly defined. For the experiment, a base value heating rate at the bottom of the tank of about 10^{-3} watt per cubic centimeter was established as typical of nuclear rocket values. The centerline nondimensional heating-rate profile closely resembled that which might be expected in a typical nuclear rocket vehicle. These parameters of heating rates and heating-rate gradient were also varied for other tests as were the flow rates.

The experimental effort was composed of three types of tests: (1) nuclear radiation flux mapping, (2) gross heat determination, and (3) flow characteristic studies. The results of the tests are reported in detail in reference 8.

Experimental Apparatus

The experimental apparatus is reported in detail in reference 8. The tank used in the series of experiments is shown in figure 2 and described in equation form in table I. The regions indicated in the table are characterized by tangent points between different geometric shapes. Also presented are equations for the cross-sectional area as a function of distance from the tank bottom.

TABLE I. - PROPELLANT TANK GEOMETRY

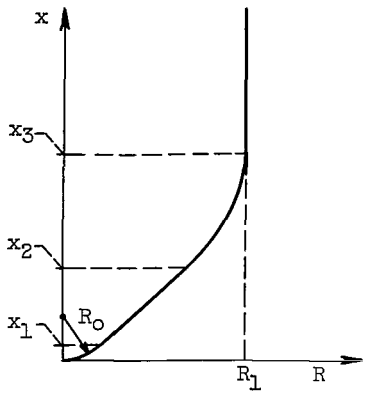

$x_1 = R_o(\sqrt{2} - 1)/\sqrt{2}$
$x_2 = k - R_1/\sqrt{2}$
$x_3 = k$
$R_o = 0.402$ ft
$R_1 = 1.333$ ft
$k = 1.719$ ft

Region[a]	Equation of tank profile	Cross-sectional area of tank	Geometry
$0 \le x \le x_1$	$R(x) = \left[R_o^2 - (x - R_o)^2\right]^{1/2}$	$A(x) = \pi(-x^2 + 2R_o x)$	Sphere
$x_1 \le x < x_2$	$R(x) = x + R_o(\sqrt{2} - 1)$	$A(x) = \pi\left[x^2 + 2R_o(\sqrt{2} - 1)x + R_o^2(\sqrt{2} - 1)^2\right]$	Cone
$x_2 \le x < x_3$	$R(x) = \left[R_1^2 - (x - k)^2\right]^{1/2}$	$A(x) = \pi\left[-x^2 + 2kx - (R_1^2 - k^2)\right]$	Sphere
$x_3 \le x \le L$	$R(x) = R_1$	$A(x) = \pi R_1^2$	Cylinder

[a]Regions are distinguished by tangent points.

The tank was mounted above the aerospace system test reactor (ASTR) at General Dynamics and was insulated to provide a maximum ambient heat leak of 50 watts. Surrounding the Dewar assembly was a liner tank that functioned as a barrier from a water shield. The shield was necessary to prevent excessive radiation exposure to personnel. The arrangement was such that the reactor could be positioned either immediately adjacent to the liner tank, reactor-tank configuration I, or separated from it with water between the two, reactor-tank configuration II. The water, by nature of its absorption properties, enabled testing with different heating-rate gradients in the liquid hydrogen and tank walls.

Platinum resistance thermometers were positioned throughout the tank to yield temperature histories in the liquid and in the ullage gas. Temperature data are presented in this report for thermometers located at 0, 15.44, 21.44, and 27.44 inches from the exit port along the tank centerline. Other types of measurements obtained include ullage pressure, liquid mass flow, liquid-level position, and radiation intensity.

Nuclear Heat Generation

A detailed knowledge of both the local and integrated or total heating-rate distribution within the propellant and in the tank walls is necessary for both applying the analysis and interpreting experimental data. The local heat generation was calculated by using a shield penetration code and was verified experimentally from measurements of neutron flux and gamma-ray dose rates. The

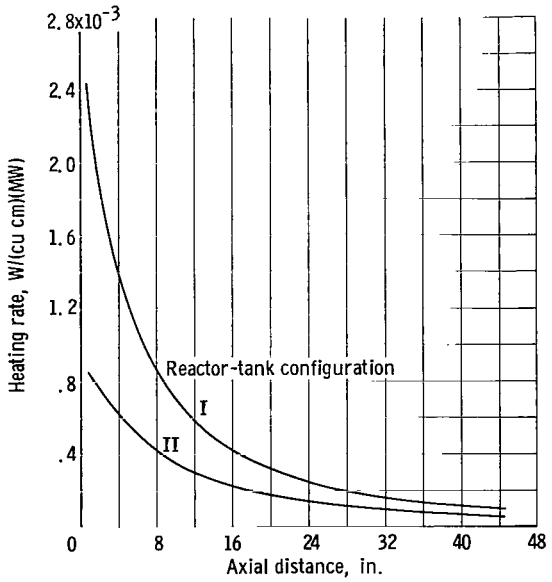

Figure 3. - Centerline heating rates in liquid hydrogen per megawatt of reactor power.

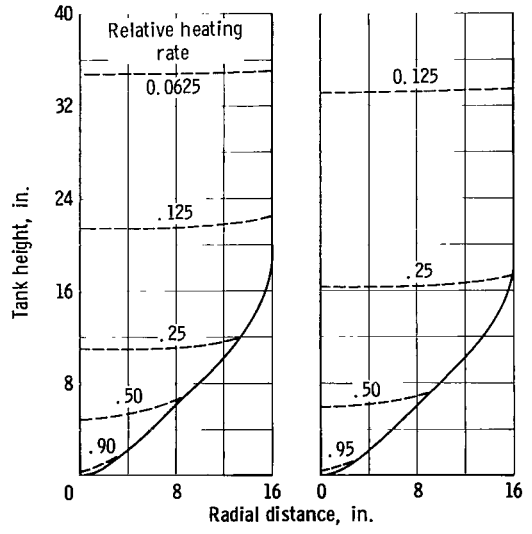

(a) Reactor-tank configuration I.

(b) Reactor-tank configuration II.

Figure 4. - Relative heating rate in hydrogen based on heating rate at tank bottom (x = 0).

manner of comparison is discussed in detail in reference 12. The integrated heat distribution was obtained both from the local heating rates and self-pressurizing data.

Calculated heating rates. - Shown in figure 3 are the calculated centerline heating rates as a function of distance into the tank for two reactor-tank configurations. The centerline heating rates calculated in reference 8 were obtained using the shield penetration program based on the differential energy spectra obtained by the moments method solution of the Boltzmann transport equation for water (ref. 13). For reactor-tank configuration I, the reactor was flush with the liner tank, while for reactor-tank configuration II, there were 4 inches of water separating the liner tank from the reactor.

Nuclear heating in a substance is primarily determined by the neutron and gamma-ray flux incident upon the configuration as well as the nature of the material itself. In hydrogeneous substances, such as liquid hydrogen, neutrons are attenuated much faster than gamma rays. For reactor-tank configuration I, the neutron and gamma ray-heating rates in the hydrogen at the bottom at the tank are about equal in magnitude, and, thus, the combined heating profile exhibits a high degree of attenuation due to the neutron contribution. By introducing a water shield between the reactor core and liner tank (reactor-tank configuration II) the neutron flux incident upon the tank bottom was reduced by a factor of 5, while the gamma-ray contribution was reduced only by a factor of 2. The elimination of much of the neutron flux incident on the tank bottom caused the heating-rate distribution for reactor-tank configuration II to assume a profile more like that of gamma rays that have less attenuation.

Shown in figure 4 are the radial heating rates for both reactor-tank configurations I and II presented in the form of lines of constant heating rate. The

heating rates shown have been normalized to the centerline heating rate at the tank bottom. For the most part, the heating rates near the wall were only slightly higher than the corresponding point along the centerline. This is true for both reactor-tank configurations I and II. Again the difference in the attenuation profile between reactor-tank configurations I and II can be seen by comparing figures 4(a) and (b).

The heat deposition within the tank walls was determined from calculations by using the shield penetration code. The validity of these calculations was determined by using them to predict the temperature rise at various points on the inner wall of the empty Dewar, taking into account heat conduction along the tank walls and leakage into the air inside the Dewar. The temperature rise determined by this method agreed reasonably well with the data.

Measured total heating rates. - Total heating rates in the liquid hydrogen were calculated for six runs during which the system was allowed to self-pressurize. Two of these runs were made without reactor power to evaluate the ambient heat leak into the hydrogen. The total heating rate per unit mass was determined from the measured temperatures by using the expression

$$q = \frac{1}{t_2 - t_1} \int_{T_1}^{T_2} c_p(T)dT$$

where $c_p(T)$ is the specific heat of the saturated vapor and $t_2 - t_1$ is the time over which the integration was done. To obtain the total heating rate, the heating rate per unit mass q was multiplied by the initial mass of fluid (since accurate measurements of the change in liquid-level position were not obtained). The calculations, however, did not constitute a rigorous heat balance, since they did not consider heat transfer across the gas-liquid interface or the work done by the expansion of the hydrogen. The results obtained by this method differ somewhat from those presented in reference 8 because the heating rate q was shown to depend on the time increment $t_2 - t_1$ over which the integration was performed. Boil-off measurements were obtained, but the flowmeter was in error, and hence these data were considered unreliable. Thus, the self-pressurizing tests were considered to represent a more reliable measure of the integrated heating rate.

Total heating rates. - The total heating rates for the system were determined by two methods: (1) integration of the calculated nuclear heating rates and (2) calculations from self-pressurizing data. The results of these two methods are shown in table II and figure 5. The total heating rates presented as a function of distance have been broken down into (1) nuclear heat generation within the hydrogen, (2) nuclear heat generation within the tank walls, and (3) ambient heat leak. The ambient heat leak was determined solely on the basis of self-pressurizing data. Ambient heating rates were obtained at two liquid levels, 27.0 and 40.7 inches from the tank bottom, and a linear distribution was assumed through the two data points. The total nuclear-heat deposition within the tank walls was determined by integration of the calculated heat-deposition rates previously described and from self-pressurizing data.

TABLE II. - TOTAL HEATING IN HYDROGEN

Reactor tank configuration	Axial distance, in.	Normalized nuclear calculations		Self-pressurizing data	
		Nuclear heating, W/MW	Wall heating, W/MW	Ambient heating, W	Nuclear plus wall heating, W/MW
I	0	0	0	----	---
	4.0	10	12	----	---
	8.0	33	23	----	---
	12.0	68	34	----	---
	16.0	101	44	----	---
	16.4	---	--	----	114
	20.0	128	52	----	---
	24.0	150	57	----	---
	26.2	---	--	28.1	---
	28.0	166	61	----	---
	32.0	179	65	----	---
	36.0	190	69	----	---
	40.0	200	73	----	---
	[a]40.7	---	--	35.3	216
	44.0	209	78	----	---
II	0	0	0	----	---
	4.0	4.0	7	----	---
	8.0	13	14	----	---
	12.0	31	21	----	---
	16.0	48	26	----	---
	20.0	64	31	----	---
	24.0	76	33	28.1	---
	26.2	---	--	----	129
	27.4	---	--	----	---
	28.0	85	36	----	---
	32.0	90	38	----	---
	[a]35.4	---	--	----	138
	36.0	101	41	----	---
	40.0	105	43	----	---
	40.7	---	--	35.3	---
	44.0	109	46	----	---

[a]Nuclear calculations normalized to self-pressurizing data at this point.

The calculated total heating rate was lower than that obtained by self-pressurizing data by about 20 percent. Most of this difference can be accounted for by the fact that the shield penetration code used could not accommodate particles with energies less than 0.1 million electron volt. Thus, the integrated nuclear-heating-rate distribution into the liquid hydrogen was obtained by first subtracting the ambient and wall-heating rates obtained at the liquid levels of 40.7 and 35.4 inches (reactor tank-configurations I and II, respectively) from the total heating obtained from self-pressurizing data at these points. The heating-rate value thus obtained was used as a basis for adjusting the calculated integrated nuclear-heat distribution within the hydrogen. The data points shown in figure 5 correspond to self-pressurizing data; the square symbol is the point of adjustment. Inasmuch as the nuclear heating in the hydrogen and in the wall are proportional to reactor power, the curves have been normalized to a reactor power of 1 megawatt. The ambient heating

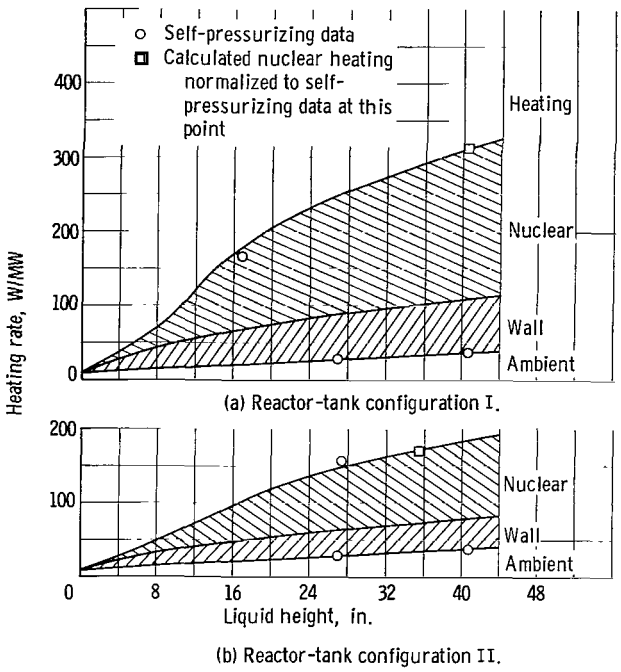

Figure 5. - Total heating in liquid hydrogen per megawatt of reactor power.

curve is independent of reactor power.

Evaluation of Other Parameters

The parameters that are associated with the experimental runs, such as average flow rate, average density, and average specific heat, etc., are defined in this section. A summary of the conditions for each of 10 experimental flow runs is presented in table III. Four additional runs were made that have not been included because they duplicate conditions presented in the other runs or because of experimental difficulties. The designated run numbers are the same as those reported in reference 8. The parameters varied in this series of experiments were reactor configuration (heat-attenuation profile), reactor power, tank pressure, and flow rate. The average flow rate presented in the table was determined from liquid-level position as a function of time as measured by thermometers and liquid-level sensors. A straight line was passed through the data, and the average flow rate was calculated from the slope of this line. As a result of the method of calculation, the average flow rates presented in table III differ slightly from those presented in reference 8. The average density and specific heat presented in table III were evaluated at the average fluid temperature defined by the relation

$$\bar{\vartheta} = \frac{\int_0^{t_f} \vartheta(0,t)\,dt}{\int_0^{t_f} dt} \tag{29}$$

where t_f is the total time to outflow. The parameters presented in table III were the same conditions that were used in the analysis.

It was experimentally shown in reference 1 that the stratification pattern is markedly affected by the presence of internal absorption of energy. The presence of internal or bottom heating caused mixing of the heated fluid along the walls with the main bulk of fluid. As yet, there is no analytical method or satisfactory experimental correlation to evaluate the degree of mixing that will occur under a given set of boundary conditions. In application, the assignment of a portion of wall heating to bulk mixing can be accomplished in the analysis

TABLE III. - EXPERIMENTAL CONDITIONS

Run	Reactor tank-configuration	Reactor power, MW	Average ullage pressure, psia	Saturation temperature difference, ϑ_s, $^{\circ}R$	Average flow rate, w_p, lb/sec	Average density, ρ, lb/cu ft	Average specific heat, c_p, Btu/(lb)($^{\circ}R$)	Initial liquid level, L, ft
14.99	I	0.492	28.5	4.00	0.0494	4.349	2.44	3.750
15.98	I	.985	59.8	9.60	.0537	4.307	2.52	3.680
16.110	I	1.065	54.0	9.00	.1309	4.357	2.43	3.530
17.108	I	3.000	55.0	8.40	.1238	4.285	2.56	3.380
18.100	I	.555	29.0	4.20	.0421	4.357	2.43	3.640
19.101	II	.985	29.4	3.64	.0539	4.340	2.46	3.450
19.110	II	1.092	34.3	5.50	.0401	4.351	2.44	3.360
20.102	II	2.175	57.0	9.60	.0394	4.287	2.55	3.480
21.102	II	1.560	58.8	9.60	.0994	4.353	2.43	3.540
22.109	II	5.720	54.0	8.50	.1248	4.299	2.53	3.600

redefining the parameters $q_w(x)$ and $q_n(x)$ that appear in equations (8) and (9) and subsequent equations. For the present comparison of analysis and experimental data, the ad hoc assumption was made that all the wall heating below the point $x = 1.125$ feet could be assigned to bulk heating. The ramifications of this assumption are discussed in detail in the section Discussion of Analytical Assumptions.

The wall-temperature parameter θ_w that appears in the expression for the exponent n (eq. (14)) was evaluated from equation 7-4a of reference 14 together with the relation

$$\bar{q}_w = h\theta_w$$

The results give

$$\theta_w = \left\{ \frac{\bar{q}_w}{0.13\, k \left[\left(\frac{c_p \mu}{k} \right) \left(\frac{g\beta}{\nu^2} \right) \right]^{1/3}} \right\}^{3/4} \tag{30}$$

where the average heat flux $\bar{q}_w$ is defined as

$$\bar{q}_w = \frac{\int q_w \, d\sigma}{\int d\sigma} \tag{31}$$

and the properties ρ and c_p were evaluated at the average field temperature defined by equation (29). It is evident that the use of equations (30) and (31) to evaluate θ_w represents a convenient approximation. The use of this approximation and its effect on analytical results will be discussed in detail

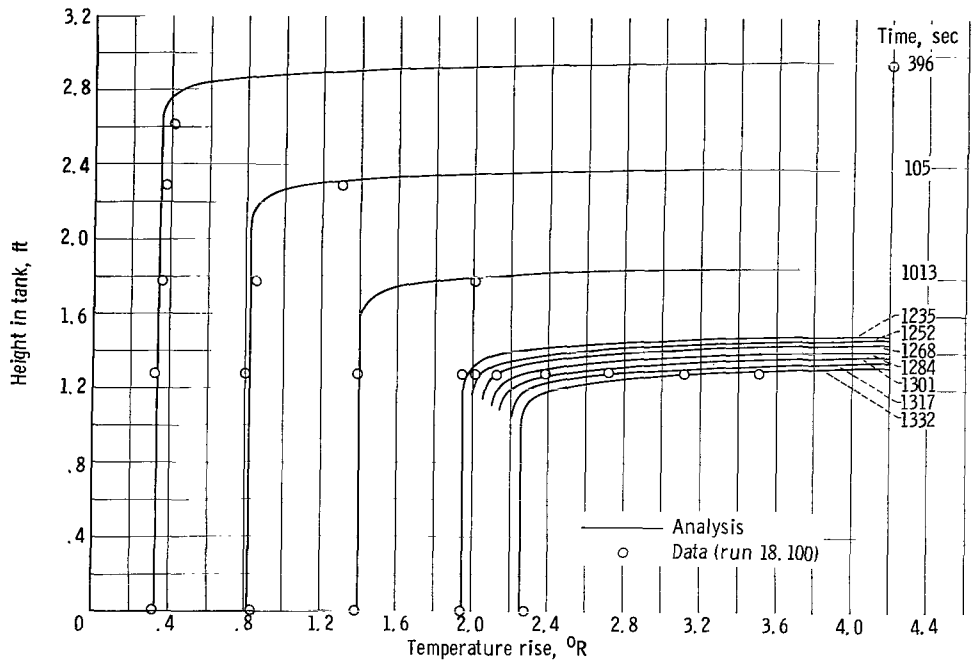

Figure 6. - Experimental and calculated temperature profiles in liquid hydrogen (run 18.100).

in the section Discussion of Analytical Assumptions.

EXPERIMENTAL AND ANALYTICAL RESULTS

The flow characteristic studies were concerned primarily with the temperature distribution in the liquid hydrogen under various conditions of (1) heating-attenuation profile, (2) total heating, (3) tank pressure, and (4) flow rate. This section deals with the comparison between the analytical and experimental results as well as interpretation of data. Typical experimental and theoretical temperature profiles in the fluid are presented in figure 6 for various times after start of flow. Experimental and calculated temperature histories for various runs are presented in figure 7.

Temperature Profiles in Hydrogen

Shown in figure 6 is a comparison between the measured and calculated temperature profiles in the fluid for run number 18.100 for various times after start of flow. The thermometers in the tank (indicated by symbols) were not spaced sufficiently close to define the temperature profile in the stratified layer accurately. By taking small time increments (as was done between 1235 and 1332 sec), however, the size of the stratified layer can be obtained approximately. It appears from the data that the stratified layer was between 3 and 4 inches thick after about 1300 seconds. The thickness of the stratified layer is considered here to be the distance, measured from the liquid surface to the point where the temperature relative to the bulk temperature becomes very small. It should be noted here that the calculations indicate that the

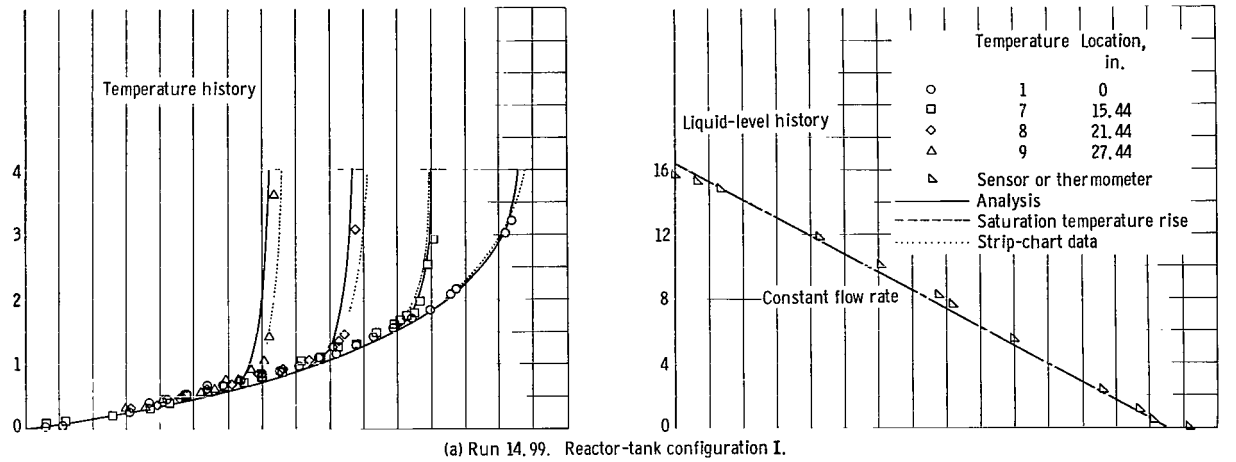

(a) Run 14.99. Reactor-tank configuration I.

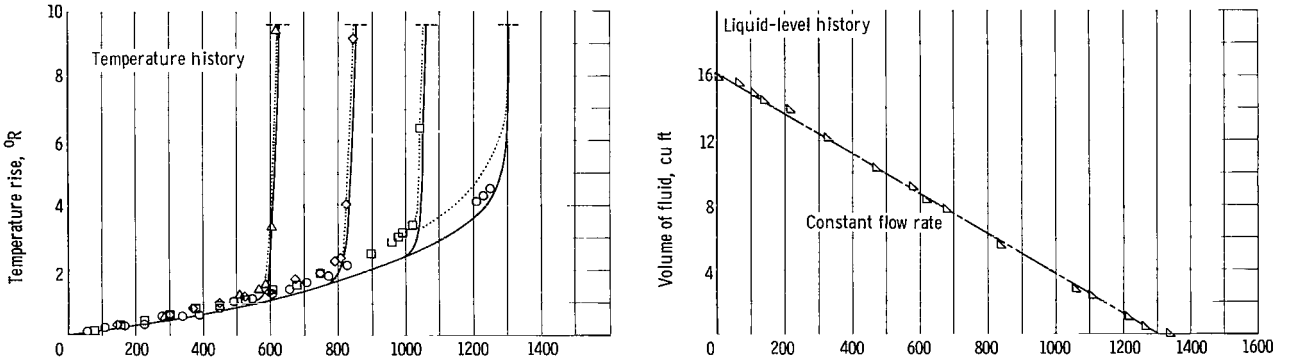

(b) Run 15.98. Reactor-tank configuration I.

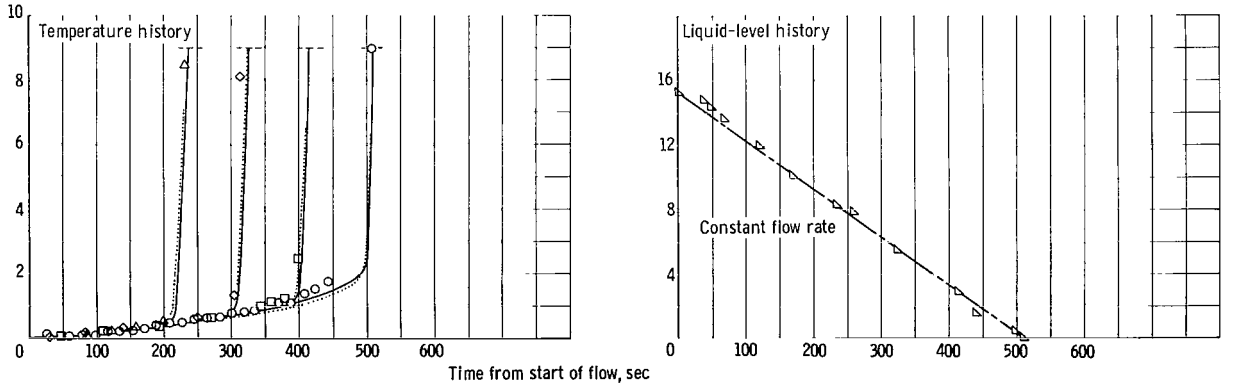

(c) Run 16.110. Reactor-tank configuration I.

Figure 7. - Temperature and liquid-level history.

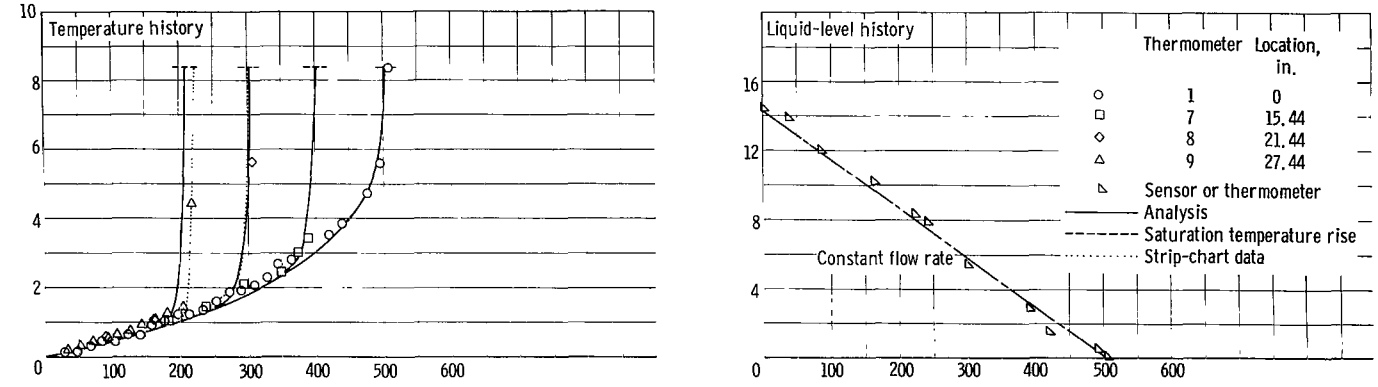

(d) Run 17.108. Reactor-tank configuration I.

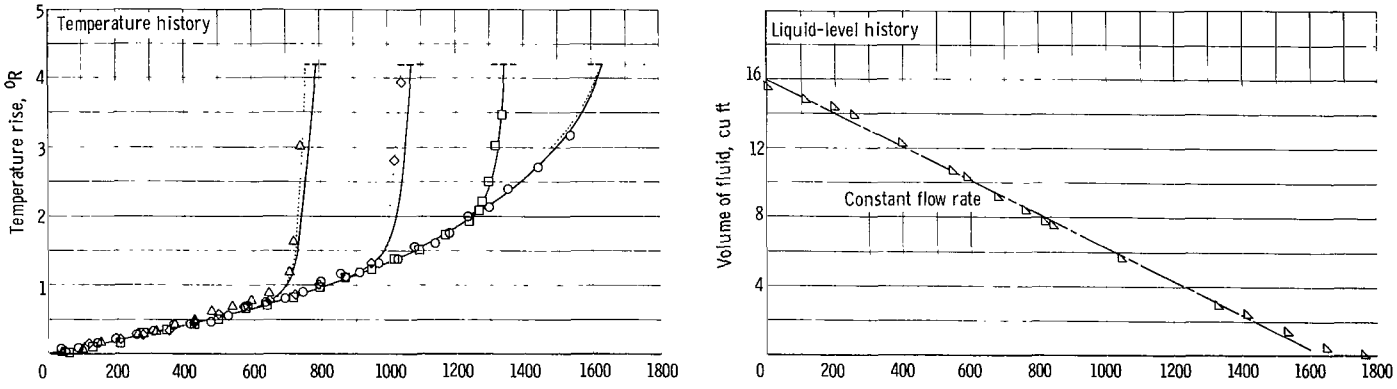

(e) Run 18.100. Reactor-tank configuration I.

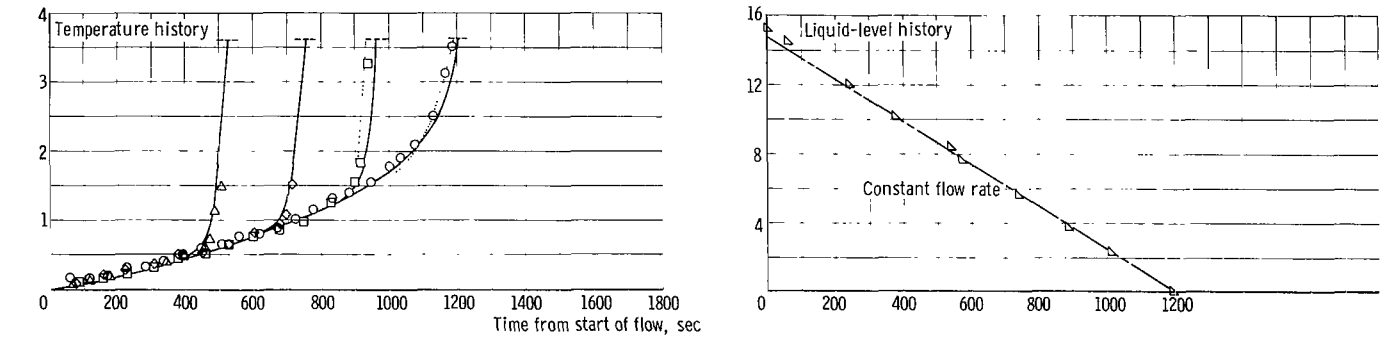

(f) Run 19.101. Reactor-tank configuration I.

Figure 7. - Continued.

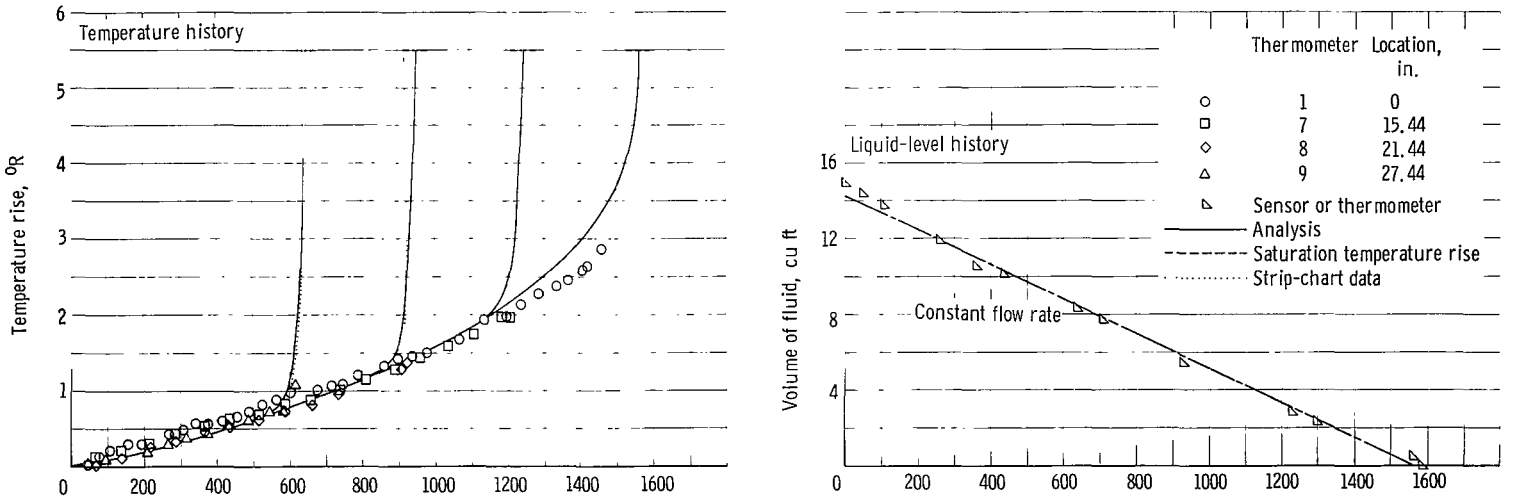

(g) Run 19.110. Reactor-tank configuration II.

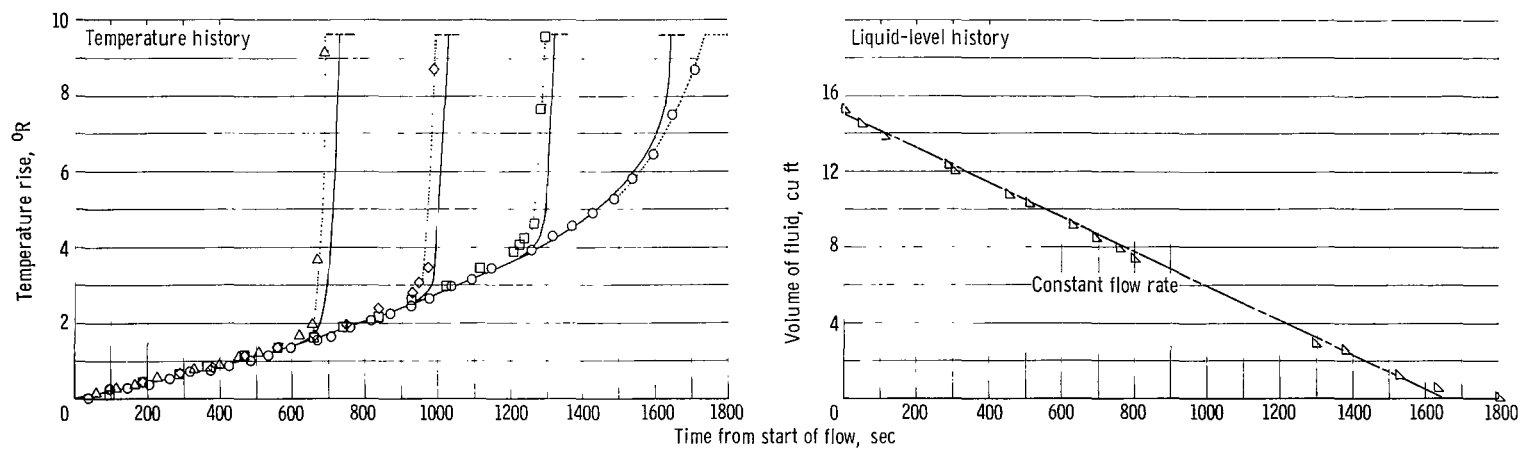

(h) Run 20.102. Reactor-tank configuration II.

Figure 7. - Continued.

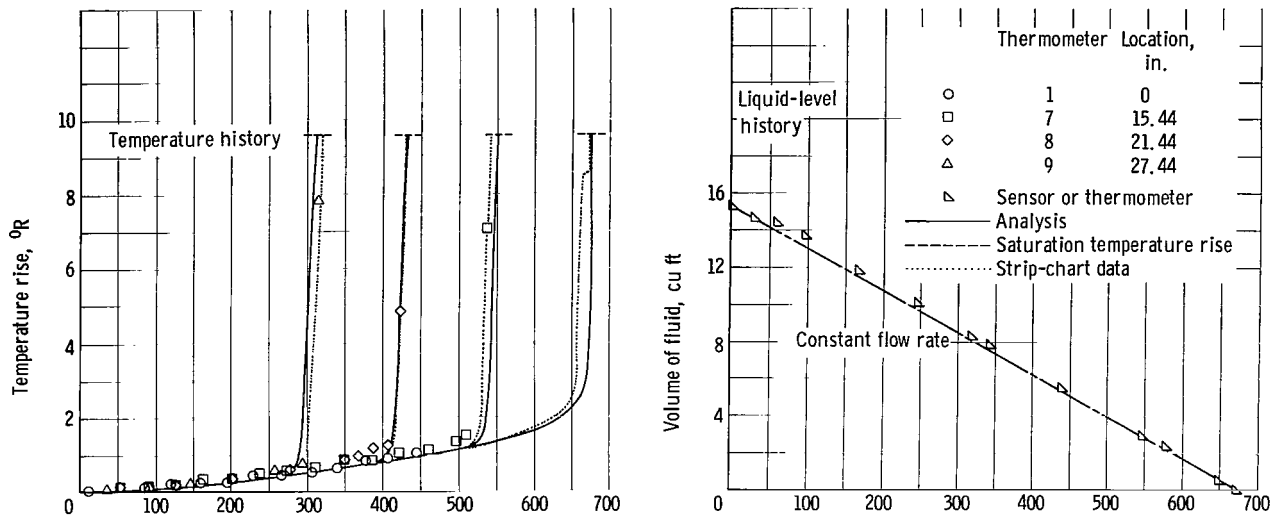

(i) Run 21.102. Reactor-tank configuration II.

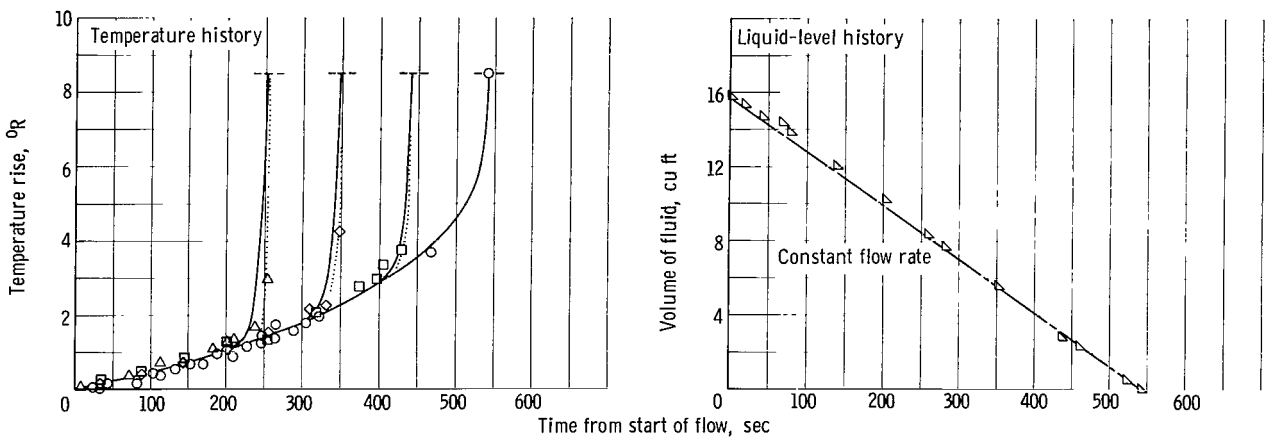

(j) Run 22.109. Reactor-tank configuration II.

Figure 7. - Concluded.

stratified layer thickness δ, as computed from equation (11), includes the entire volume of fluid remaining in the tank after 396 seconds. Because the temperature rapidly approaches its bulk value (due to the high value of the exponent n), however, this large thickness can not be seen in figure 6. This phenomenon can also be seen in the results presented in reference 1 by comparing the Schlieren photographs showing the transient formation of convective currents for wall heating alone with the measured temperature profiles. It appears that there is a relatively loose coupling between the velocity and temperature field in the fluid; thus, the parameter δ is not a good indication of the stratified layer thickness.

Experimental Temperature Histories

The data presented in figure 7 show the temperature histories of the fluid at axial positions 0, 15.44, 21.44, and 27.44 inches from the tank bottom. The

dashed line indicates the temperature rise necessary to achieve saturation at each height. Over the range of experimental conditions set for this study, the temperature rise indicated by the thermometers at each position showed only a relatively thin stratified layer at the liquid surface. This is indicated by the fact that all the sensors read the same temperature just prior to any one leaving the fluid. This can be accounted for, in part, by the fact that a great deal of mixing occurs between the bounding region of the main bulk and stratified layer. This phenomenon was observed in the small-scale infrared tests reported in reference 1 and can be seen from Schlieren photographs and temperature data presented therein.

It can be seen by comparing figures 7(a) and (b) for reactor-tank configuration I and figures 7(g) and (h) for reactor-tank configuration II that the bulk temperature rise is approximately proportional to reactor power. The effects of tank pressure are thus seen to occur primarily within the relatively thin stratified layer that is formed at the gas-liquid interface. The effect of the water shield between the reactor core and liner tank (i.e., the effects of changing the heating-rate profile) can be seen by a comparison of figures 7(e) and (f). The reactor power for reactor-tank configuration II (fig. 7(f)) was about twice that of reactor-tank configuration I (fig. 7(e)), while all other parameters were about the same. A comparison of the temperature history of the fluid up to about 800 seconds shows that the bulk temperature rise from the initial value is about the same. This indicates that the bulk temperature rise was governed primarily by the total heating of the system and was relatively insensitive to the centerline heating profiles (fig. 3, p. 15). The insensitivity of the temperature history to the heating profile was due to the small volume of fluid in the vicinity of the tank bottom as a consequence of tank geometry. Increasing the flow rate and keeping the other input parameters approximately the same tended to effect an increase in the bulk temperature rise for the same corresponding time from start of flow. This increase may be due, in part, to the fact that the higher flow rate caused the region of uniform mixing to decrease at a faster rate. In general, there were no gross changes in the flow behavior from those observed in reference 1.

Calculated Temperature Histories

The heating-rate-input curves presented in figure 5, the equations of the tank geometry presented in table I, and the test conditions in table III were used in the analysis to predict local temperature histories with reasonable accuracy, as shown in figure 7. Because the experimental flow rate was not held entirely constant, there are differences between the analysis and the experimental data for the time required to indicate the saturation temperature rise for some thermometers. For example, consider thermometer 8 in figure 7(a). The data indicate that the saturation temperature was reached about 990 seconds from the start of flow, while the analysis predicts about 960 seconds based on a constant flow rate. This type of difference between data and analysis became apparent for thermometer 1 near the end of some runs because of a sharp drop in flow rate (e.g., figs. 7(a), (e), and (h)). To give some indication of the temperature history, where data from the digital voltmeter were unavailable, temperature data from continuous strip-chart recordings were obtained. These data are plotted as dotted lines. In some of the runs, (e.g., fig. 7(e)),

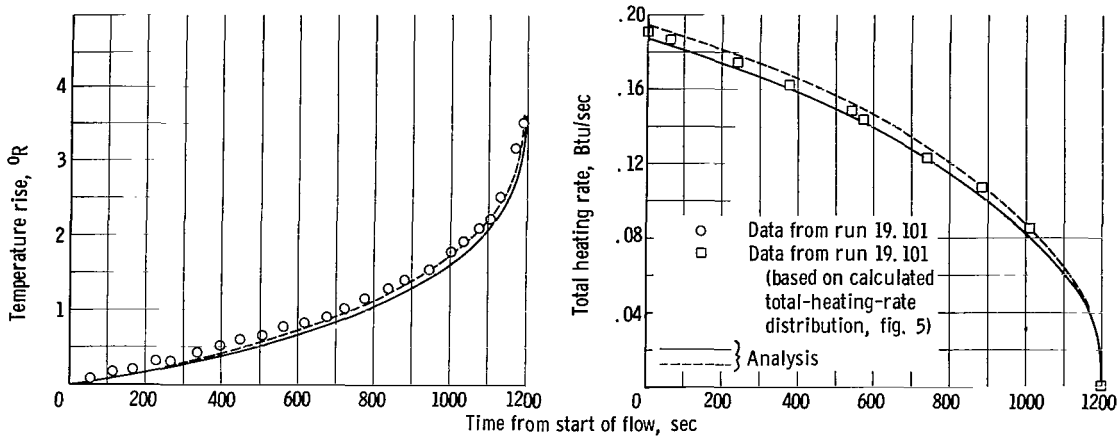

(a) Temperature history.

(b) Total-heating-rate history.

Figure 8. - Effect of total-heating-rate history on temperature history.

saturation temperature rise was reached prior to the end of the flow run. After the saturation temperature was reached, the strip-chart data indicated a period of constant (saturation)temperature. For run 18.100, (fig. 7(e)) this period lasted about 130 seconds, which indicated that the fluid was boiling.

In general, the analysis tended to underestimate the temperature rise in fluid for a given time after the start of flow either because of an underestimation of the heating-rate distribution (fig. 5, p. 18) or because of errors in the input variables density ρ, specific heat c_p, and mass flow rate $\dot{w}_p$ used in the calculations. The errors associated with the latter are discussed in the next section.

In order to determine the effects of perturbations of the total heating-rate history on the temperature history at the tank exit, the total-heating-rate input to the analysis was arbitrarily varied. The results of this perturbation study are shown in figure 8, which presents the temperature histories (fig. 8(a)), for the two total-heating-rate histories (solid and dashed lines shown in fig. 8(b)). Also shown in the figure are temperature-time data for run 19.101 and the total heating rate based on the measured liquid level and heating-rate profile presented in figure 5. The data always fall between the solid and dashed lines in the total-heating-rate history (fig. 8(b)); however, the temperature data generally fall above the dashed line (fig. 8(a)). The small but apparent inconsistency between the heating-rate-input data and the temperature history could occur because of one or more of the following reasons:

(1) Differences could occur in the heating-rate curves themselves because mass and energy transfer across the gas-liquid interface and work rate of compression effects were not considered in reducing the self-pressurizing data.

(2) Accumulative error could have arisen in the IBM 7094 computer program used in the analysis as a result of numerical integration.

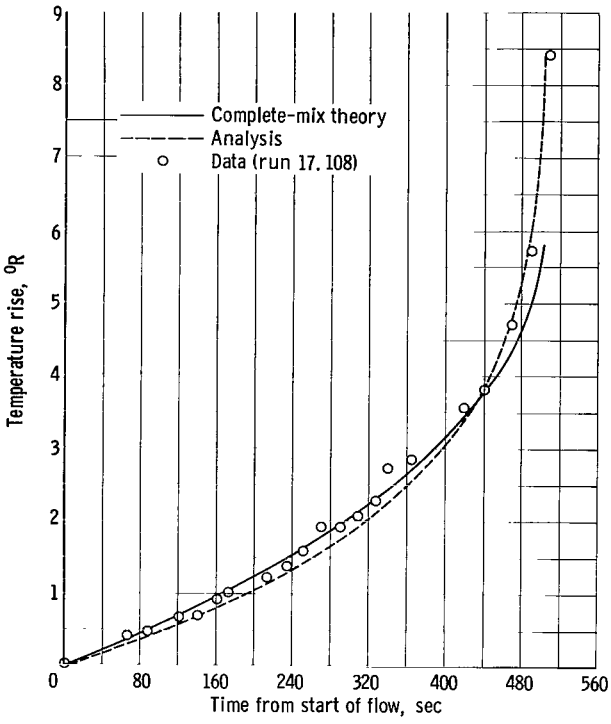

Figure 9. - Comparison of complete-mix theory and analysis.

(3) The temperature data may have been influenced by the radiation field along with perturbations in the fluid.

Comparisons Between Flow Models

Shown in figure 9 is a comparison between the temperature history of the tank exit for the assumption that the incoming heat is distributed uniformly over the volume of fluid (complete-mix theory), indicated by the solid line, and the temperature history determined from the analysis, indicated by the dashed line. Data are also presented and are indicated by the symbols. The effect of wall heating on what the pump experiences is clearly seen in figure 9. During the earlier portion of the run, the complete-mix calculations indicate a higher temperature than the present analysis because a lower portion of the heat is stored at the liquid surface. Consequently, near the end of the run, the analysis predicts a higher temperature rise than that indicated by complete-mix theory. The effect of bottom or nuclear heating is thus seen to distribute more of the heat in the earlier portion of the run and less near the end. This phenomenon may provide a mechanism whereby the severity of temperature stratification in the liquid can be reduced.

Although the temperature histories computed by the two methods are relatively close, differences can be realized depending on the vehicle mission. For example, if the temperature rise (based on fig. 9) is limited to 5.5° R, comparison of the solid and dashed lines shows that approximately 4 percent of the propellant is unusable. If, however, a 4-percent outage is admitted, then the temperature rise will be higher by about 0.75° R than that computed by complete-mix theory.

Parametric Study

The summary of conditions presented in table II (p. 17) represents a parametric study of the variations in reactor-tank configuration (heating profiles), reactor power, flow rate, and tank pressure. Since the proper parameters could not be held entirely constant between different runs, a parametric study was performed using the analysis to make the comparisons more definitive.

The results of a parametric study obtained from the analysis are presented in figures 10 and 11. Comparisons are made by using the heating-rate-input data for reactor-tank configurations I and II from figure 5 (p. 18). Figure 10

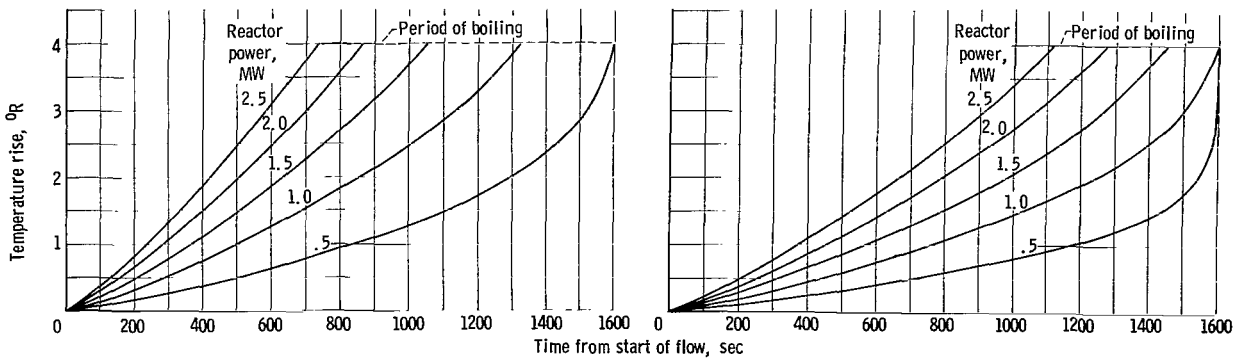

(a) Reactor-tank configuration I.

(b) Reactor-tank configuration II.

Figure 10. - Effect of reactor power (total heating) on temperature history at tank exit. Fluid mass flow rate, 0.04 pound per second; saturation temperature difference, 4.0° R.

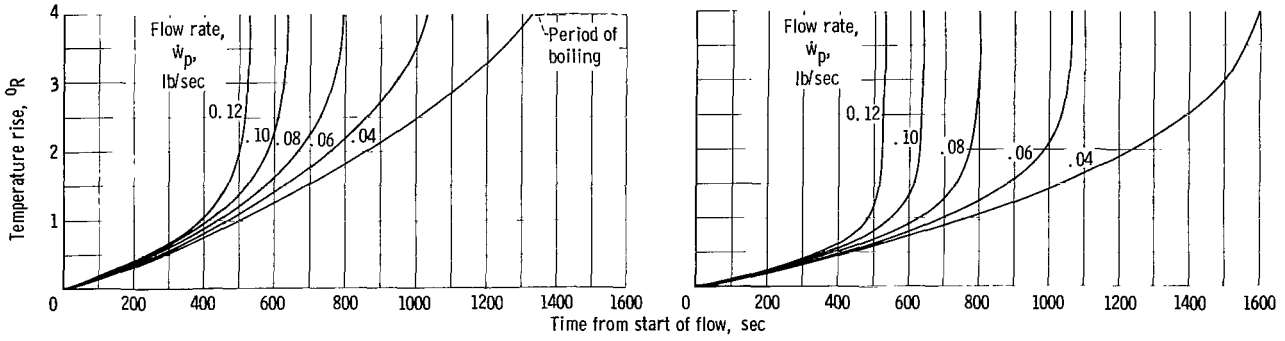

(a) Reactor-tank configuration I.

(b) Reactor-tank configuration II.

Figure 11. - Effect of flow rate on temperature history at exit port. Reactor power, 1 megawatt. Saturation temperature difference, 4.0° R.

shows the effects of varying the reactor power, where the flow rate was held fixed at 0.04 pound per second and ϑ_s was held fixed at 4.0° R. The reactor power was varied from 0.5 to 2.5 megawatts. In general, the temperature rise of the fluid was approximately proportional to reactor power up to about 500 seconds, after which differences appeared. The dashed portions of the curves indicate where the analysis predicted the occurrence of boiling. During this period, the fluid temperature remains nearly constant at a saturation temperature corresponding to the ullage pressure. In a full-scale vehicle, boiling prior to full fluid discharge represents unusable propellant. Comparison of figures 10(a) and (b) shows the effect of a 4-inch water shield between the reactor and tank. At 1 megawatt of reactor power 4 inches of water shield sufficiently reduced the incident flux on the tank to increase the usable propellant by about 18 percent.

Figure 11 shows the effect of liquid flow rate on the temperature rise at the tank exit where the reactor power was fixed at 1 megawatt and ϑ_s was 4° R. The flow rate was varied from 0.04 to 0.12 pound per second. For short times, there was an increase in the temperature rise with increased flow rate at a given time. This was observed in the experimental data discussed previously. The effect of the 4-inch water shield can again be seen by comparing figures 11(a) and (b). At a flow rate of 0.06 pound per second and a reactor power of 1 megawatt, an increase of about 3.7 percent of usable propellant was

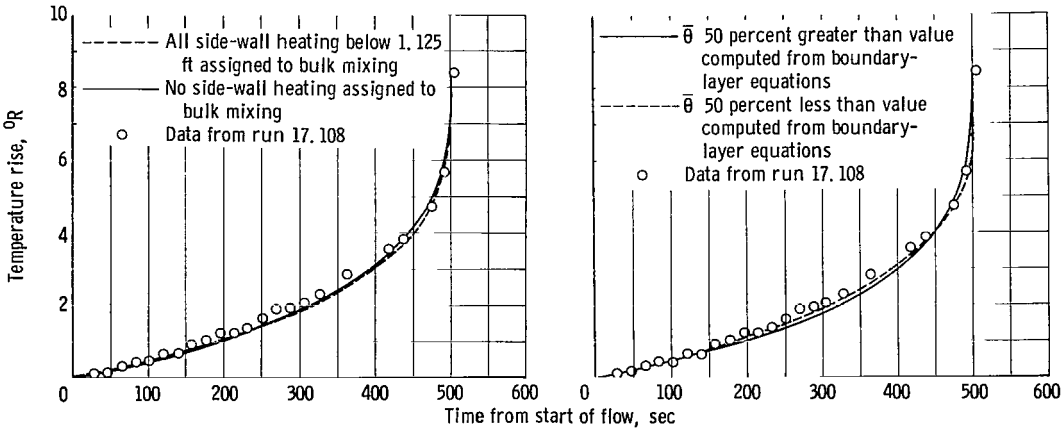

(a) Deviations resulting from apportionment of side-wall heating to bulk mixing.

(b) Deviations resulting from average temperature $\bar{\theta}$ of fluid entering stratified layer.

Figure 12. - Effect of analytical assumptions on temperature history at tank exit.

realized with the water shield. This compares with 18 percent for a flow rate of 0.04 pound per second at a reactor power of 1 megawatt. The primary effect of increasing the tank pressure was to inhibit boiling in the fluid, as would be expected, and thus the curves were not presented.

Discussion of Analytical Assumptions

The process of free convection within a confined fluid subjected to the internal absorption of energy is extremely complex and not entirely understood. Because exact solutions to this problem are presently not available, simplifying assumptions must be made to obtain approximate solutions. It is not readily apparent, however, that these assumptions are entirely justified. To some extent they can be verified by experimental data.

The original form of the similarity profile (see eq. (2)) does not represent a unique solution for the temperature distribution within the fluid. In view of the reasonable agreement between data and analysis, within the range of experimental conditions, however, it was concluded that the profile assumed is a good representation of the fluid temperature profile when nuclear or internal absorption of energy is present. It should be pointed out that the original concept of a similarity temperature profile in the fluid is a basic assumption and should be investigated further, but it appears to be a useful tool to obtain engineering quantities.

Assigning an arbitrary portion of wall heating to bulk mixing, which is synonymous with assuming a starting position for the boundary layer, represents an apparent source of error that cannot go unchallenged. To determine the degree of deviation that will result, the amount of wall heating assigned to bulk mixing was varied. Figure 12(a) presents the results obtained by apportionment of all the wall heating below $x = 1.125$ feet to bulk mixing (dashed line) and no wall heating to bulk mixing (solid line). The comparisons were made from data obtained from run 17.108 and are typical of results obtained for

different runs. The results indicated that no serious error was incurred by the the assignment of wall heating to bulk mixing for the range of experimental conditions presented.

The insensitivity of the analysis to the amount of wall heating assigned to to bulk mixing may be the result of two reasons: (1) the nature of the heating-rate-input curves (fig. 5 p. 18) and (2) the natural consequence of the assumption of similarity (eq. (2)). It can be seen from equation (2) that, when the bulk-heating contribution to the temperature profile is increased, the wall-heating contribution is decreased, thus tending to minimize any variations.

To investigate the basic assumption of treating the flow along the side walls as representing a boundary-layer flow, whose character is the same as known flat-plate solutions, the parameter $\overline{\theta}$, which is related to the wall heat-transfer rate, was varied ±50 percent of the value computed from equations (13), (30), and (31). The subsequent results and comparison with data are shown in figure 12(b). The solid line indicates a $\overline{\theta}$ 50 percent greater, and the dashed line shows a $\overline{\theta}$ 50 percent less than the values computed from boundary-layer equations. The results indicate a relatively small difference in predicting the temperature rise within the range of the experimental conditions. The apparent insensitivity of the analysis to the use of the flat-plate boundary-layer solution may be due, in part, to the relative values of wall and nuclear heating considered in this report.

SUMMARY OF RESULTS

The following results were obtained from an analytical and experimental study of the development of thermal stratification in liquid hydrogen contained in a tank exposed to nuclear radiation.

1. A portion of the nuclear heat generated within the tank walls caused convective motion within the liquid hydrogen that carried warm fluid to the liquid surface. The warm fluid accumulated near the gas-liquid interface and produced a temperature gradient or stratified layer.

2. In general, no gross changes in the flow behavior were observed over the range of experimental conditions.

3. The technique of assuming a similarity temperature profile that is made to satisfy conservation of energy gave analytical results that were in reasonable agreement with experimental measurements.

4. Within the range of experimental conditions, no major errors were found by using flat-plate boundary-layer approximations in the analytical formulation.

5. Under those conditions where internal heat generation was present, no appreciable error was incurred by the inability to define the boundary-layer starting position accurately.

Lewis Research Center,
National Aeronautics and Space Administration,
Cleveland, Ohio, April 20, 1965.

APPENDIX A

SYMBOLS

$A(x)$	cross-sectional area
$a(x_s)$	parameter defined by eq. (15)
$b(x_s)$	parameter defined by eq. (16)
c_p	specific heat per unit mass
$F(x_s)$	parameter defined in eq. (18)
$f(x_s)$	parameter defined in eq. (5)
$G(x_s)$	parameter defined by eq. (27)
Gr_{x_o}	Grashof numbers based on x_o
g	acceleration due to gravity
H_1	parameter defined by eq. (B12)
H_2	parameter defined by eq. (B13)
h	heat-transfer coefficient
I_1	parameter defined by eq. (B7)
I_2	parameter defined by eq. (B8)
k	thermal conductivity
L	initial liquid level
m	mass entering stratified layer
n	parameter defined by eq. (14)
Pr	Prandtl number
$Q(x_s)$	parameter defined by eq. (28)
$Q_n(x_s)$	parameter defined by eq. (23)
$Q_w(x_s)$	parameter defined by eq. (22)
q	heating rate per unit mass

$q_n(x)$	nuclear heat deposition
$q_w(x)$	wall heat flux
r	radial coordinate
R	tank radius
T	temperature
t	time
u	velocity in boundary layer relative to wall
u_1	velocity outside boundary layer of comparable forced-convection flow
$\bar{u}$	velocity in entire fluid relative to wall
$\dot{w}_p$	mass flow rate of fluid
x	axial distance measured from tank bottom
y	coordinate normal to tank wall
$\alpha(x_s)$	parameter defined by eq. (25)
β	coefficient of thermal expansion
$\Gamma(n)$	gamma function
$\gamma(x_s)$	parameter defined by eq. (26)
Δ	boundary-layer thickness
$\delta(x_s)$	stratified-layer thickness
$E(x)$	parameter defined by eq. (D4)
ϵ	ratio of boundary-layer thickness to tank radius
η	dimensionless coordinate normal to wall
θ	temperature difference in boundary flow, $T(y) - T_b(t)$
ϑ	temperature difference $T(x,t) - T_i$
μ	viscosity
ν	kinematic viscosity
ρ	density

σ surface area of tank

$\Phi(x,t)$ parameter defined by eq. (20)

$\varphi(x,t)$ parameter defined by eq. (6)

$\Psi(x,t)$ parameter defined by eq. (19)

$\psi(x,t)$ parameter defined by eq. (6)

Subscripts:

b bulk conditions

i initial conditions

n nuclear-heating contribution

o lower extremity of stratified layer

s surface conditions

s,ℓ limiting conditions

w wall-heating conditions

Superscripts:

(*) dimensionless quantities

$(\bar{\ })$ average value

APPENDIX B

EVALUATION OF MASS AND ENERGY FLUX

For a steady incompressible flow, conservation of mass can be written as

$$\int_0^R \bar{u} r \, dr = 0 \tag{B1}$$

where $\bar{u}$ is the velocity distribution across the tank. Let u_o be the velocity at which the stratified layer moves. Equation (B1) can thus be written as

$$\int_0^R u_o r \, dr + \int_0^R (\bar{u} - u_o) r \, dr = 0$$

The mass flux entering the stratified layer can thus be written as

$$\frac{dm}{dt} = 2\pi\rho \int_0^R u_o r \, dr = -2\pi\rho \int_0^R (\bar{u} - u_o) r \, dr \tag{B2}$$

Equation (B2) can also be written as

$$\frac{dm}{dt} = 2\pi\rho \int_{R-\Delta}^R (u + u_o) r \, dr - 2\pi\rho \int_0^{R-\Delta} (u_b - u_o) r \, dr$$

where u is the velocity distribution in the boundary layer and u_b is the velocity distribution in the main bulk. The velocity u_o will be defined as

$$u_o = \frac{\int_0^{R-\Delta} u_b r \, dr}{\int_0^{R-\Delta} r \, dr}$$

Hence the mass flux becomes

$$\frac{dm}{dt} = 2\pi\rho \int_{R-\Delta}^R (u + u_o) r \, dr \tag{B3}$$

Likewise the energy flux can be written as

$$\frac{d}{dt}\left(c_p \theta m\right) = 2\pi\rho c_p \int_{R-\Delta}^{R} \theta(u + u_o) r \, dr \tag{B4}$$

Introducing the transformation $y = R - r$ and using the definition of u_o yields the expression for conservation of mass

$$u_o \int_{\Delta}^{R} (R - y)dy = \int_{0}^{\Delta} u(R - y)dy \tag{B5}$$

Integrating the left side of equation (B5) gives

$$u_o \int_{\Delta}^{R} (R - y)dy = \frac{u_o R^2}{2}\left[1 - \left(\frac{\Delta}{R}\right)\right]^2$$

The integral on the right side of equation (B5) can be evaluated by introducing the dimensionless quantities

$$\eta = \frac{y}{\Delta}$$

$$u^* = \frac{u}{u_1}$$

$$\theta^* = \frac{\theta}{\theta_w}$$

Thus,

$$\int_{0}^{\Delta} u(R - y)dy = u_1 R^2 \left[\left(\frac{\Delta}{R}\right) \int_{0}^{1} u^* \, d\eta - \left(\frac{\Delta}{R}\right)^2 \int_{0}^{1} u^* \eta \, d\eta\right]$$

Setting

$$\epsilon = \frac{\Delta}{R} \tag{B6}$$

$$I_1 = \int_{0}^{1} u^* \, d\eta \tag{B7}$$

$$I_2 = \int_{0}^{1} u^* \eta \, d\eta \tag{B8}$$

and assuming $\epsilon \ll 1$ give the velocity u_o as

$$u_o = 2u_1\left[\epsilon + \epsilon^2(2 - \epsilon) + \epsilon^3(2 - \epsilon)^2 + \ldots\right] I_1 - 2u_1\left[\epsilon^2 + \epsilon^3(2 - \epsilon) + \epsilon^4(2 - \epsilon)^2 + \ldots\right] I_2 \quad \text{(B9)}$$

From equation (B3),

$$\frac{dm}{dt} = 2\pi\rho \int_0^{\Delta} (u + u_o)(R - y)dy = 2\pi\rho \left(R \int_0^{\Delta} u\, dy - \int_0^{\Delta} uy\, dy + Ru_o \int_0^{\Delta} dy - \int_0^{\Delta} y\, dy\right)$$

Introducing the dimensionless parameters gives the mass flux:

$$\frac{dm}{dt} = 2\pi\rho u_1 R^2(\epsilon I_1 - \epsilon^2 I_2) + 2\pi\rho u_o R^2 \frac{\epsilon}{2}(2 - \epsilon)$$

Using equation (B9) results in

$$\frac{dm}{dt} = 2\pi\rho u_1 R^2 \epsilon\left[I_1 + \epsilon(2I_1 - I_2) + \epsilon^2(3I_1 - 2I_2) + \ldots\right] \quad \text{(B10)}$$

Likewise, the energy flux can be written as

$$\frac{d}{dt}(c_p\theta m) = 2\pi\rho c_p \theta_w R^2 \epsilon\left[H_1 + \epsilon(2H_1 - H_2) + \epsilon^2(3H_1 - 2H_2) + \ldots\right] \quad \text{(B11)}$$

where

$$H_1 = \int_0^1 \theta^* u^*\, d\eta \quad \text{(B12)}$$

$$H_2 = \int_0^1 \theta^* u^* \eta\, d\eta \quad \text{(B13)}$$

Using the free-convection profiles for turbulent flow along a flat plate (ref. 5), that is,

$$u = u_1 \eta^{1/7}(1 - \eta)^4$$

$$\theta = \theta_w(1 - \eta^{1/7})$$

gives equations (B10) and (B11) in the form

$$\frac{dm}{dt} = 2\pi\rho u_1 R^2 \epsilon(0.1464 + 0.2654\ \epsilon + 0.3844\ \epsilon^2 + 0.5034\ \epsilon^3 + \ldots) \qquad \text{(B14)}$$

$$\frac{d}{dt}(c_p \theta m) = 2\pi\rho c_p u_1 \theta_w R^2 \epsilon(0.0366 + 0.0612\ \epsilon + 0.0858\ \epsilon^2 + 0.1104\ \epsilon^3 + \ldots)$$
$$+ 0.1104\ \epsilon^3 + \ldots\ldots\ldots\ldots) \qquad \text{(B15)}$$

the value of ϵ can be determined from equation (24) of reference 5; that is,

$$\epsilon = \frac{\Delta}{x_o} \cdot \frac{x_o}{R} = 0.565(Gr_{x_o})^{-1/10}(Pr)^{-8/15}\left[1.0 - 0.494(Pr)^{2/3}\right]^{-1/10} \cdot \frac{x_o}{R} \qquad \text{(B16)}$$

where R is evaluated at $x = x_o$.

APPENDIX C

EVALUATION OF INTEGRALS IN INITIAL PERIOD

Consider

$$b(x_s) = \frac{d}{dx_s} \int_0^{x_s} \psi(x,x_s)A(x)dx \tag{C1}$$

By virtue of the fact that the nuclear and wall contributions were uncoupled in the energy equation (see eq. (8))

$$\frac{d}{dx_s} \int_0^{x_s} \psi(x,x_s)A(x)dx = -Q_w(x_s) \tag{C2}$$

where $Q_w(x_s)$ is defined by equation (22). Thus

$$b(x_s) = -Q_w(x_s) \tag{C3}$$

Integrating equation (B2) with the initial condition that $x_s = L$ at $t = 0$ yields

$$\int_0^{x_s} \psi(x,x_s)A(x)dx = \int_{x_s}^{L} Q_w(x_s)dx_s \tag{C4}$$

From equation (15),

$$a(x_s) = \int_0^{x_s} A(x)dx - \int_{x_s}^{L} Q_w(x_s)dx_s \tag{C5}$$

APPENDIX D

EVALUATION OF INTEGRALS IN LATER PERIOD

Consider the integral

$$I = \int_a^b \Psi(x,x_s)A(x)dx \tag{D1}$$

Substituting the expression for $\Psi(x,x_s)$ from equation (19)

$$I = \int_a^b \left[1 - \left(\frac{x_s - x}{x_{s,l}}\right)\right]^n A(x)dx \tag{D2}$$

By successive integration by parts, equation (D2) becomes

$$I = \left\{\frac{x_{s,l}}{(n+1)}\left[1 - \left(\frac{x_s - x}{x_{s,l}}\right)\right]^{n+1} A(x) - \frac{x_{s,l}^2}{(n+1)(n+2)}\left[1 - \left(\frac{x_s - x}{x_{s,l}}\right)\right]^{n+2} \frac{dA}{dx}\right.$$

$$\left. + \frac{x_{s,l}^3}{(n+1)(n+2)(n+3)}\left[1 - \left(\frac{x_s - x}{x_{s,l}}\right)\right]^{n+3} \frac{d^2A}{dx^2} - \cdots\right\}\Bigg|_a^b \tag{D3}$$

If the area can be expressed as a polynomial of finite degree d, equation (D3) would have a finite number of terms. Defining the parameter $E(x)$ yields

$$E^{n+p}(x) \equiv \frac{\Gamma(n+1)x_{s,l}^p}{\Gamma(n+p+1)}\left[1 - \left(\frac{x_s - x}{x_{s,l}}\right)\right]^{n+p} \qquad p = 1,2 \cdots \tag{D4}$$

where $\Gamma(n+1)$ and $\Gamma(n+p+1)$ are gamma functions. Then equation (D3) becomes

$$I = \left\{\sum_{p=1}^{d+1} (-1)^{p+1} E^{n+p}(x) \frac{d^{p-1}}{dx^{p-1}}\left[A(x)\right]\right\}\Bigg|_a^b \tag{D5}$$

where the zeroth order derivative is understood to mean

$$\frac{d^o}{dx^o}\left[A(x)\right] = A(x)$$

Consider now the derivative of equation (D1), that is,

$$\frac{dI}{dx_s} = \frac{d}{dx_s} \int_0^b \Psi(x,x_s)A(x)dx \tag{D6}$$

By using equation (D5)

$$\frac{dI}{dx_s} = \frac{d}{dx_s} \left\{ \sum_{p=1}^{d+1} (-1)^{p+1} E^{n+p}(x) \frac{d^{p-1}}{dx^{p-1}} \left[A(x)\right] \Bigg|_a^b \right\} \tag{D7}$$

but

$$\frac{d}{dx_s} \left[E^{n+p}(x)\right] = -E^{n+p-1}(x)$$

Therefore, if $b \neq x_s$

$$\frac{dI}{dx_s} = \left\{ \sum_{p=1}^{d+1} (-1)^{p} E^{n+p-1}(x) \frac{d^{p-1}}{dx^{p-1}} \left[A(x)\right] \right\} \Bigg|_a^b \tag{D8}$$

If $b = x_s$,

$$\frac{dI}{dx_s} = \sum_{p=1}^{d+1} (-1)^{p+1} \frac{\Gamma(n+1)x_s^p, l}{\Gamma(n+p+1)} \frac{d^p}{dx_s^p} \left[A(x_s)\right]$$

$$+ \sum_{p=1}^{d+1} (-1)^{p+1} E^{n+p-1}(x) \frac{d^{p-1}}{dx^{p-1}} \left[A(x)\right] \Bigg|_{x=a} \tag{D9}$$

REFERENCES

1. Anderson Bernhard H.; and Kolar, Michael J.: Experimental Investigation of the Behavior of a Confined Fluid Subjected to Nonuniform Source and Wall Heating. NASA TN D-2079, 1963.

2. Tatom, J. W.; Brown, W. H.; Knight, L. H.; and Coxe, E. F.: Analysis of Thermal Stratification of Liquid Hydrogen in Rocket Propellant Tanks. Vol. 9 of Advances in Cryogenic Eng., Plenum Press, 1964, pp. 265-272.

3. Robbins, J. H.; and Rogers, A. C., Jr.: An Analysis Predicting Thermal Stratification in Liquid Hydrogen. Paper No. 64-426, AIAA, 1964.

4. Vliet, G. C.: Stratified Layer Flow Model: A Numerical Approach to Temperature Stratification in Liquids Contained in Heated Vessels. Aerospace Sci. Lab., Lockheed Missiles and Space Co., Nov. 1964.

5. Eckert, E. R. G.; and Jackson, Thomas W.: Analysis of Turbulent Free-Convection Boundary Layer on Flat Plate. NACA Rept. 1015, 1951.

6. Clark, John A.: A Review of Pressurization, Stratification and Interfacial Phenomena. Paper Presented at Cryogenic Eng. Conf., Univ. Penn., Aug. 18-21, 1964.

7. Anderson, B. H.; Huntley, S. C.; and Connolley, D. J.: Propellant Heating Studies with Wall and Nuclear Heating. Paper Presented at ASME Meeting, New York (N.Y.), Nov. 29-Dec. 4, 1964.

8. Hehs, W. A.; McCauley, B. O.; Miller, G. E.; and Wheeler, D. M.: Nuclear Radiation Heating in Liquid Hydrogen. NASA CR-54078, Vol. I and II, 1964.

9. Ostrach, Simon (With appendix B by Lynn U. Albers): An Analysis of Laminar Free-Convection Flow and Heat Transfer About a Flat Plate Parallel to the Direction of the Generating Body Force. NASA Rept. 1111, 1953.

10. Ostrach, S.: Laminar Flows with Body Forces. Vol. IV of High Speed Aerodynamics and Jet Prop., Princeton Univ. Press, 1964.

11. Gluck, D. F.; and Kline, J. F.: Gas Requirements in Pressurized Transfer of Liquid Hydrogen. Vol. 7 of Advances in Cryogenic Engineering, K. D. Timmerhaus, ed., Plenum Press, 1962, pp. 219-233.

12. Hehs, W. A.; and Miller, G. E.: Measured and Calculated Nuclear Radiation Distributions in Liquid Hydrogen. NASA CR-54003, 1964.

13. Peterson, D. M.: Shield Penetration Programs C-17 and L-63. Rept. No. FZK 9-170 (NARF-61-39T), General Dynamics/Fort Worth, Dec. 1961.

14. McAdams, William H.: Heat Transmission. Third ed., McGraw-Hill Book Co., Inc., 1954.

2/22/95
58

"The aeronautical and space activities of the United States shall be conducted so as to contribute . . . to the expansion of human knowledge of phenomena in the atmosphere and space. The Administration shall provide for the widest practicable and appropriate dissemination of information concerning its activities and the results thereof."

—NATIONAL AERONAUTICS AND SPACE ACT OF 1958

NASA SCIENTIFIC AND TECHNICAL PUBLICATIONS

TECHNICAL REPORTS: Scientific and technical information considered important, complete, and a lasting contribution to existing knowledge.

TECHNICAL NOTES: Information less broad in scope but nevertheless of importance as a contribution to existing knowledge.

TECHNICAL MEMORANDUMS: Information receiving limited distribution because of preliminary data, security classification, or other reasons.

CONTRACTOR REPORTS: Technical information generated in connection with a NASA contract or grant and released under NASA auspices.

TECHNICAL TRANSLATIONS: Information published in a foreign language considered to merit NASA distribution in English.

TECHNICAL REPRINTS: Information derived from NASA activities and initially published in the form of journal articles.

SPECIAL PUBLICATIONS: Information derived from or of value to NASA activities but not necessarily reporting the results of individual NASA-programmed scientific efforts. Publications include conference proceedings, monographs, data compilations, handbooks, sourcebooks, and special bibliographies.

Details on the availability of these publications may be obtained from:

SCIENTIFIC AND TECHNICAL INFORMATION DIVISION

NATIONAL AERONAUTICS AND SPACE ADMINISTRATION

Washington, D.C. 20546